Development of Correlations for Overall Gas Hold-up, Volumetric Mass Transfer Coefficient, and Effective Interfacial Area in Bubble Column Reactors Using Hybrid Genetic Algorithm-Support Vector Regression Technique: Viscous Newtonian and Non-Newtonian Liquids

Prashant P. Gupta,[†] Shamel S. Merchant,[†] Akshay U. Bhat,[†] Ankit B. Gandhi,[†] Sunil S. Bhagwat,[†] Jyeshtharaj B. Joshi,*[,†] Valadi K. Jayaraman,[‡] and Bhaskar D. Kulkarni[‡]

Institute of Chemical Technology, University of Mumbai, Matunga, Mumbai 400 019, India, and Chemical Engineering and Process Development Division, National Chemical Laboratory, Pune 411008, India

The objective of this study was to develop hybrid genetic algorithm−support vector regression (GA-SVR)-based correlations for overall gas hold-up (ϵ_G), volumetric mass-transfer coefficient ($k_L\underline{a}$), and effective interfacial area ($\underline{a}$) in bubble column reactors for gas−liquid systems employing viscous Newtonian and non-Newtonian systems as the liquid phase. The hybrid GA-SVR is a novel technique based on the feature generation approach using genetic algorithm (GA). In the present study, GA has been used for nonlinear rescaling of attributes. These, exponentially scaled, are eventually subjected to SVR training. The technique is an extension of conventional SVR technique, showing relatively enhanced results. For this purpose an extensive literature search was done. From the published literature, 1629 data points for viscous Newtonian and 845 data points for viscous non-Newtonian systems for ϵ_G, 500 data points for viscous Newtonian and 556 data points for viscous non-Newtonian systems for $k_L\underline{a}$, and 208 data points for viscous non-Newtonian systems for $\underline{a}$, respectively, were collected. These data sets were collected spanning the years 1965−2007. Correlations were developed after taking into account all the parameters affecting ϵ_G, $k_L\underline{a}$, and $\underline{a}$ such as column and sparger geometry, gas−liquid properties, operating temperature, pressure, and superficial gas and liquid velocities. The correlations thus developed gave prediction accuracies of 0.994 and 0.999 and average absolute relative errors (AARE) of 3.75 and 1.65% for viscous Newtonian and non-Newtonian systems for ϵ_G, prediction accuracies of 0.983 and 0.998 and AARE of 8.62 and 1.91% for viscous Newtonian and non-Newtonian systems for $k_L\underline{a}$, and prediction accuracy of 0.999 and AARE of 1% for viscous non-Newtonian systems for $\underline{a}$, respectively. These correlations also showed much improved results when compared with all the existing correlations proposed in literature. To facilitate their usage, all the hybrid GA-SVR-based correlations have been uploaded on the web link http://www.esnips.com/web/UICT-NCL.

1. Introduction

Gas−liquid-based multiphase contacting is widely encountered commercially for conducting prominent chemical reactions such as oxidation, hydrogenation, chlorination, halogenation, hydrohalogenation, ammonolysis, alkylation, polymerization, fermentation, Fischer−Tropsch synthesis, and biological wastewater treatment processes, etc. Among various multiphase contactors devised, bubble columns are the most widely used as they offer high rates of heat and mass transfer, require less maintenance due to the absence of moving parts, and occupy less floor space and, hence, are less expensive. Bubble columns are also easier to operate. In view of widespread usage, the design and scale-up of these columns thus become extremely important. The three most important parameters which govern the performance of bubble columns are as follow: overall gas hold-up (ϵ_G), volumetric mass-transfer coefficient ($k_L\underline{a}$), and effective interfacial area ($\underline{a}$).

ϵ_G is one of the most important parameters defining the hydrodynamics of bubble columns. On one hand it defines the gas-phase volume present in the reactor and thus the gas-phase residence time. On the other hand, ϵ_G along with the knowledge of mean bubble diameter helps in determining $\underline{a}$. Third, the value of ϵ_G and its radial and axial profiles govern the flow pattern in bubble columns. The knowledge of $k_L\underline{a}$ and $\underline{a}$ is needed in estimating the rates of mass transfer.

Among various media used for carrying out chemical reaction in bubble columns, viscous media (Newtonian and non-Newtonian) are frequently encountered in food processing, pharmaceutical, and other biotechnological applications. Viscous media having coalescing tendency tend to form large bubbles in the bubble column. Relatively high bubble rise velocity associated with large bubbles causes a decrease in the bubble residence time, hence decreasing ϵ_G thus resulting into a decrease in $\underline{a}$ and $k_L\underline{a}$. Thus, it becomes extremely important to capture the relevant hydrodynamics and mass-transfer rates existing in the column when viscous liquids are being used. This is possible only if correct correlations are used for the estimation of ϵ_G, $k_L\underline{a}$, and $\underline{a}$ for viscous media. To date, the correlations published in literature deviate significantly from experimental values when used for predictions outside the range of experiments on which they were originally devised.[1] In view of such a status of knowledge, it is the objective of this study to propose correlations for better predictions of ϵ_G, $k_L\underline{a}$, and $\underline{a}$ in bubble column reactors for gas−liquid systems using viscous liquid media by making use of data-driven modeling techniques.

Data-driven modeling techniques have been finding increasing relevance and usage in development of correlations for chemically reacting systems. Among them, artificial neural networks

* To whom all the correspondence should be addressed. Tel.: +91-22-4145616. Fax: +91-22-4145614. E-mail: jbj@udct.org.
[†] University of Mumbai.
[‡] National Chemical Laboratory.

10.1021/ie801834w CCC: $40.75

Table 1. Summary of Correlations for Overall Gas Hold-up for Viscous Newtonian Systems

researcher	correlation		range
	(A) Newtonian System		
Akita and Yoshida[11]	$\left(\frac{\epsilon_G}{(1-\epsilon_G)^4}\right) = 0.2(Bo)^{1/8}(Ga)^{1/2}(Fr)$	(1)	
Bach and Pilhofer[13]	$\left(\frac{\epsilon_G}{1-\epsilon_G}\right) = 0.115\left(\frac{V_G{}^3\rho_L{}^2}{g\mu_L(\rho_L-\rho_G)}\right)^{0.23}$	(2)	valid only for pure liquids and cannot be used for aqueous solutions or mixtures
Hikita et al.[14]	$\epsilon_G = 0.672\left(\frac{V_G\mu_L}{\sigma_L}\right)^{0.578}\left(\frac{\mu_L{}^4 g}{\rho_L\sigma_L{}^3}\right)^{-0.131}\left(\frac{\rho_G}{\rho_L}\right)^{0.062}\left(\frac{\mu_G}{\mu_L}\right)^{0.107}$	(3)	$1.1\times10^{-3} < (V_G\mu_L/\sigma_L) < 8.9\times10^{-2}$, $2.5\times10^{-11} < (\mu_L{}^4 g/\rho_L\sigma_L{}^3) < 1.9\times10^{-6}$, $8.4\times10^{-5} < (\rho_G/\rho_L) < 1.9\times10^{-2}$, $0.001 < (\mu_G/\mu_L) < 0.018$
Godbole et al.[16]	$\epsilon_G = 0.319 V_G{}^{0.476}\mu_L{}^{-0.058}$	(4)	
Koide et al.[12]	$\left(\frac{\epsilon_G}{(1-\epsilon_G)^4}\right) = 0.277\left(\frac{V_G\mu_L}{\sigma_L}\right)^{0.918}\left(\frac{g\mu_L{}^4}{\rho_L\sigma_L{}^3}\right)^{-0.252}$	(5)	valid for heterogeneous regime
Sotelo et al.[15]	$\epsilon_G = 129\left(\frac{V_G\mu_L}{\sigma_L}\right)^{0.99}\left(\frac{\mu_L{}^4 g}{\rho_L\sigma_L{}^3}\right)^{-0.123}\left(\frac{\rho_G}{\rho_L}\right)^{0.187}\left(\frac{\mu_G}{\mu_L}\right)^{0.343}\left(\frac{d_0}{D}\right)^{-0.089}$	(6)	valid for d_0 in the range of $(30-150)\times10^{-6}$ m
Joshi et al.[1]	$\epsilon_G = 0.62 V_G{}^{0.56}\left(\frac{\sigma_W}{\sigma_L}\right)^{0.15}\left(\frac{\mu_W}{\mu_L}\right)^{0.15}\left(\frac{\rho_G}{\rho_a}\right)^{0.15}\left(\frac{\rho_W}{\rho_L}\right)^{0.15}$	(7)	valid for $D > 0.15$ m, $H_L/D > 5$, $V_G > 0.08$ m/s
Anabtawi et al.[17]	$\epsilon_G = 0.66 V_G{}^{0.6}\mu_L{}^{-0.24}H_L{}^{-0.38}\sigma_L{}^{0.22}\rho_L{}^{0.02}$	(8)	valid for $0.0018 < V_G < 0.29$ m/s, $0.12 < H_L < 0.6$ m, $0.063 < \mu_L < 0.32$ Pa s, $906 < \rho_L < 928$ kg/m^3, $0.0248 < \sigma_L$ s < 0.035 N/m
Urseanu et al.[18]	$\epsilon_G = 0.21 V_G{}^{0.58}D^{-0.18}\mu_L{}^{-0.12}\rho_G{}^{[0.3\exp(-9\mu_L)]}$	(9)	valid for $0.05 < \mu_L < 0.55$ Pa s
Kazakis et al.[19]	$\epsilon_G = 0.2\left[\left(\frac{V_G{}^2}{D}\right)^{0.8}\left(\frac{D^3\rho_L{}^2 g}{\mu_L{}^2}\right)^{0.2}\left(\frac{D^2\rho_L g}{\sigma_L}\right)^{1.6}\left(\frac{d_s}{D}\right)^{0.9}\left(\frac{d_0}{d_s}\right)^{0.03}\right]^{2/5}$	(10)	valid for d_0 in the range of $(40-100)\times10^{-6}$ m
	(B) Non-Newtonian System		
Godbole et al.[16]	$\epsilon_G = 0.225 V_G{}^{0.532}\mu_{eff}{}^{-0.146}$	(11a)	valid for $0.023 < \mu_{eff} < 0.23$ Pa s
	$\epsilon_G = 0.239 V_G{}^{0.634}D^{-0.5}$	(11b)	valid for $D \le 0.3$ m
Schumpe and Deckwer[34]	$\epsilon_G = 0.0908 V_G{}^{0.85}$	(12a)	valid for homogeneous regime $0.07 < \mu_{eff} < 2.64$ Pa s
	$\epsilon_G = 0.0322 V_G{}^{0.674}$	(12b)	valid for slug flow regime $0.07 < \mu_{eff} < 2.64$ Pa s
Godbole et al.[31]	$\epsilon_G = 0.207 V_G{}^{0.6}\mu_{eff}{}^{-0.19}$	(13)	
Devine et al.[35]	$\epsilon_G = 0.528 V_G{}^{0.635}$	(14)	valid for $0.07 \le V_G \le 0.41$ m/s

Table 1. Continued

researcher	correlation		range
Haque et al.[38]	$\epsilon_G = 0.171 V_G^{0.6}[k(5000V_G)^{n-1}]^{-0.22} D^{-0.15}$	(15)	valid for $0.1 \le D \le 1$ m, $0.0003 \le d_0 \le 0.002$ m, $V_G \ge 0.03$ m/s and is valid for the heterogeneous regime
Kawase and Moo-Young[36]	$\epsilon_G = 0.24 n^{-0.6}(Fr)^{(0.84-0.14n)}(Ga)^{0.07}$	(16)	valid for $0.008 \le V_G \le 0.285$ m/s, $0.14 \le D \le 0.35$ m, $0.28 \le n \le 1$, $0.001 \le k \le 1.22$ Pa s^n
Kawase et al.[37]	$\epsilon_G = 1.07 n^{2/3}\left(\frac{V_G^2}{gD}\right)^{1/3}$	(17)	
Schumpe and Deckwer[40]	$\epsilon_G = 0.2(Bo)^{-0.13}(Ga)^{0.11}(Fr)^{0.54}$	(18)	$1.4 \times 10^3 \le Bo \le 1.4 \times 10^5$, $1.2 \times 10^7 \le Ga \le 6.5 \times 10^{10}$. $3 \times 10^{-3} \le Fr \le 2.2 \times 10^{-1}$
Vatai and Tekic[39]	$\epsilon_G = 0.19 n^{-0.6}(Fr)^{(0.84-0.14n)}(Ga)^{0.07}$	(19a)	valid for $0.002 < V_G < 0.1$
	$\epsilon_G = 0.19 V_G^{0.534} D^{-0.5}$	(19b)	valid for slug flow regime
Fransolet et al.[32]	$\epsilon_G = 0.26 V_G^{0.54} \mu_{eff}^{-0.147}$	(20)	
Lakota[33]	$\epsilon_G = 0.0524 V_G^{0.623} \mu_{eff}^{-0.0531}$	(21a)	valid for systems operated batchwise wrt liquid phase
	$\epsilon_G = 0.0485 V_G^{0.666} \mu_{eff}^{-0.1181}$	(21b)	valid for systems operated continuously wrt liquid phase

Table 2. Summary of Correlations for Effective Interfacial Area for Viscous Non-Newtonian Systems

researcher	correlation		range
Schumpe and Deckwer[34]	$\underline{a} = 0.0465 V_G^{0.51} \mu_{eff}^{-0.51}$	(22)	valid for heterogeneous regime
Godbole et al.[31]	$\underline{a} = 19.2 V_G^{0.47} \mu_{eff}^{-0.76}$	(23)	valid for heterogeneous regime
Popovic and Robinson[48]	$\underline{a} = 233 V_G^{0.83} \mu_{eff}^{-0.327}$	(24)	valid for heterogeneous regime
Kawase et al.[37]	$\underline{a} = 0.399 n^{1.85}\left(\frac{V_G^{0.73} g^{0.23} \rho_L^{0.6}}{\sigma_L^{0.6} D^{0.16}}\right)$	(25)	

(ANN) is the most commonly and widely used data-driven modeling technique. For modeling of the parameters for bubble column reactors, ANN has been already employed by Xie et al.[2] for classification of the flow regime in multiphase flows, while in context to design it has been used by Shaikh and Al-Dahhan[3] for correlating the overall gas hold-up in bubble column reactors. Recently, support vector regression (SVR) rigorously based on statistical learning theory data is gaining popularity for driven modeling. SVR uses structural risk minimization; hence, it accounts for model complexity as well as minimizes training data error, while ANN makes use of empirical risk minimization which minimizes training data error only. Additionally SVR provides globally minimal solutions. Moreover, SVR allows computations in the input space itself, thus avoiding cumbersome calculations. Apart from this, SVR also defines regression function with better generalization capability, provides robust solutions, and allows sparseness of regression function thus describing the function with a limited number of support vectors (subset of training data). SVR has been successfully employed by Desai et al.[4] in fed-batch bioreactors for soft sensor development and by Gandhi et al.[5] for correlating ϵ_G in bubble column reactors for various gas−liquid systems.

In recent years, use of genetic algorithm (GA) has become very common to the field of medical diagnosis[6] and fault diagnosis.[7] GAs have been used in conjunction with SVR to find an optimum set of SVR model parameters,[8] in the field of process modeling[9] and reactor design.[10] In this study, GA has been used for nonlinear rescaling of attributes. This is done by raising each feature to an optimal power value before employing them as input features with SVR. The conventional linear scaling

Table 3. Summary of Correlations for Volumetric Mass-Transfer Coefficient for Viscous Newtonian and Non-Newtonian Systems

researcher	correlation		range
	(A) Newtonion System		
Akita and Yoshida[11]	$\frac{k_L a D^2}{D_L} = 0.6(Sc)^{0.5}(Bo)^{0.62}(Ga)^{0.31}\epsilon_G^{1.1}$	(26)	
Nakanoh and Yoshida[49]	$\frac{k_L a D^2}{D_L} = 0.09(Sc)^{0.5}(Bo)^{0.75}(Ga)^{0.39}(Fr)$	(27)	
Hikita et al.[50]	$\frac{k_L a V_G}{g} = 14.9\left(\frac{V_G \mu_L}{\sigma_L}\right)^{1.76}\left(\frac{\mu_L^4 g}{\rho_L \sigma_L^3}\right)^{-0.246}\left(\frac{\mu_G}{\mu_L}\right)^{0.243}\left(\frac{\mu_L}{\rho_L D_L}\right)^{-0.604}$	(28)	$5 \times 10^{-4} < (V_G\mu_L/\sigma_L) < 3.3 \times 10^{-2}$, $120 < (\mu_L/\rho_L D_L) < 20000$, $1.3 \times 10^{-11} < (\mu_L^4 g/\rho_L \sigma_L^3) < 3.2 \times 10^{-7}$, $0.0016 < (\mu_G/\mu_L) < 0.025$
Koide et al.[12]	$\frac{k_L a \sigma_L}{\rho_L D_L g} = 2.11(Sc)^{0.5}\left(\frac{g\mu_L^4}{\rho_L \sigma_L^3}\right)^{-0.159}\epsilon_G^{1.18}$	(29)	
Kawase and Moo-Young[36]	$\frac{k_L a D^2}{D_L} = 6.8(Re)^{0.9}(Sc)^{0.52}$	(30)	$0.008 < V_G < 0.084$ m/s, $0.14 < D < 0.305$ m, $0.00089 < \mu_L < 2.82$ Pa s
Schumpe and Deckwer[40]	$Sh = 0.021(Sc)^{0.5}(Bo)^{0.21}(Ga)^{0.6}(Fr)^{0.49}$	(31)	$5.4 \times 10^3 < Sh < 1.8 \times 10^6$, $2.2 \times 10^3 < Sc < 2.3 \times 10^5$, $1.2 \times 10^5 < Ga < 1.1 \times 10^{10}$, $4.9 \times 10^2 < Bo < 1.2 \times 10^4$, $0.014 < Fr < 0.25$
Kawase et al.[37]	$\frac{k_L a D^2}{D_L} = 0.447(Sc)^{0.5}(Re)^{3/4}(Fr)^{7/60}(Bo)^{3/5}$	(32)	
Ozturk et al.[51]	$\frac{k_L a d_B^2}{D_L} = 0.62(Sc)^{0.5}(Bo)^{0.33}(Ga)^{0.29}(Fr)^{0.68}\left(\frac{\rho_G}{\rho_L}\right)^{0.04}$	(33)	$16 \le (k_L a d_B^2/D_L) \le 970$, $32 \le Sc \le 1.5 \times 10^5$, $1.2 \le Bo \le 5.4$, $830 \le Ga \le 1.5 \times 10^6$, $0.043 \le Fr \le 0.6$, $9.3 \times 10^{-5} \le (\rho_G/\rho_L) \le 2 \times 10^{-3}$.
Terasaka and Tsuge[24]	$\frac{k_L a D^2}{D_L} = 6.34(Sc)^{0.5}(Bo)^{0.559}(Ga)^{0.261}(Fr)^{0.526}N_0^{0.313}$	(34)	$3.93 \times 10^6 \le Sc \le 3.06 \times 10^{10}$, $1.4 \times 10^3 \le Bo \le 8.67 \times 10^3$, $1.24 \times 10^6 \le Ga \le 1.11 \times 10^{11}$, $4.13 \times 10^{-7} \le Fr \le 3.31 \times 10^{-4}$, $7 \le N_0 \le 331$
Sotelo et al.[15]	$\frac{k_L a V_G}{g} = 16.9\left(\frac{V_G \mu_L}{\sigma_L}\right)^{2.14}\left(\frac{\mu_L^4 g}{\rho_L \sigma_L^3}\right)^{-0.518}\left(\frac{\mu_G}{\mu_L}\right)^{0.074}(Sc)^{-0.038}\left(\frac{d_0}{D}\right)^{0.908}$	(35)	valid for d_0 in the range $(30-150) \times 10^{-6}$ m; for $150 \times 10^{-6} \le d_0 \le 200 \times 10^{-6}$ and $k_1 = 1.924$; for $90 \times 10^{-6} \le d_0 \le 150 \times 10^{-6}$ and $k_1 = 1.969$; for $40 \times 10^{-6} \le d_0 \le 90 \times 10^{-6}$ and $k_1 = 2.079$
Alvarez et al.[53]	$k_L a = k_1 V_G^{2/3}\mu_L^{-3/4}\rho_L^{3/2}\sigma_L^{3/4}$	(36)	valid for $8.5 \times 10^{-4} \le V_G \le 1.5 \times 10^{-3}$ m/s, $997 \le \rho_L \le 1030$ kg/m^3, $0.896 \times 10^{-3} \le \mu_L \le 1.135 \times 10^{-3}$ Pa s, $0.0652 \le \sigma_L \le 0.073$, $1.55 \times 10^{-9} \le D_L \le 1.897 \times 10^{-9}$
Lau et al.[54]	$k_L a = 1.77\sigma_L^{-0.22}e^{(1.65V_L - 65.3\mu_L)}\epsilon_G^{1.2}$	(37)	
	(B) Non-Newtonian System		
Nakanoh and Yoshida[49]	$\frac{k_L a D^2}{D_L} = 0.09(Sc)^{0.5}(Bo)^{0.75}(Ga)^{0.39}(Fr)(1 + 0.13De^{0.55})^{-1}$	(38)	
Deckwer et al.[42]	$k_L a = 0.000208 V_G^{0.59}\mu_{eff}^{-0.84}$	(39)	valid for slug flow regime
Godbole et al.[31]	$k_L a = 0.000835 V_G^{0.44}\mu_{eff}^{-1.01}$	(40)	valid for churn-turbulent regime

Table 3. Continued

researcher	correlation		range
Kawase and Moo-Young[36]	$\frac{k_L a D^2}{D_L} = 6.8 n^{-6.72} (Re)^{(0.38n+0.52)} (Sc)^{(0.38n+0.14)}$	(41)	valid for $0.008 < V_G < 0.084$ m/s, $0.14 < D < 0.35$ m, $0.543 < n < 1$, $0.00089 < k < 2.82$ Pa s^n
Kawase et al.[37]	$\frac{k_L a D^2}{D_L} = 0.4518 n^{1.83} \left(\frac{k D^{1-n}}{\rho_L D V_G^{1-n}}\right)^{0.5} \left(\frac{\rho_L D^n V_G^{2-n}}{k}\right)^{(2+n)/(2+2n)} (Fr)^{(11n-4)/(30n+30)} (Bo)^{3/5}$	(42)	
Schumpe and Deckwer[40]	$\frac{k_L a D^2}{D_L} = 0.021 (Sc)^{0.5} (Bo)^{0.21} (Ga)^{0.6} (Fr)^{0.49}$	(43)	$5.4 \times 10^3 < (k_L a D^2/D_L) < 1.8 \times 10^6$; $2.2 \times 10^3 < Sc < 2.3 \times 10^5$, $1.2 \times 10^5 < Ga < 1.1 \times 10^{10}$, $4.9 \times 10^2 < Bo < 1.2 \times 10^4$, $0.014 < Fr < 0.25$
Popovic and Robinson [45]	$k_L a = 0.005 V_G^{0.52} D_L^{0.5} \rho_L^{1.03} \mu_{eff}^{-0.89} \sigma_L^{-0.75}$	(44)	$0.14 \le V_L \le 0.35$ m/s, $0.03 \le V_G \le 0.26$ m/s, $0.02 \le \mu_{eff} \le 0.5$ Pa s, $0.33 \times 10^{-9} \le D_L \le 2.53 \times 10^{-9}$ m^2/s, $1003 \le \rho_L \le 1240$ kg/m^3, $0.059 \le \sigma_L \le 0.079$ N/m
Vatai and Tekic[39]	$\frac{k_L a D^2}{D_L} = 0.0308 (Sc)^{0.5} (Bo)^{0.39} (Fr)$	(45)	
Suh et al.[59]	$\frac{k_L a D^2}{D_L} = 0.018 (Sc)^{0.5} (Bo)^{0.2} (Ga)^{0.62} (Fr)^{0.51} (1 + 0.12 Wi)^{-1}$	(46)	$6.25 \times 10^3 \le (k_L a D^2/D_L) \le 2.31 \times 10^6$, $1.73 \times 10^3 \le Sc \le 2.27 \times 10^5$, $0 \le Wi \le 41.4$, $491 \le Bo \le 1.4 \times 10^4$, $2.05 \times 10^5 \le Ga \le 1.07 \times 10^{10}$, $0.14 \le Fr \le 0.4$
Merchuk and Ben-Zvi[56]	$k_L a = 1.4 \times 10^{-6} \gamma_l^{1.7}$	(47)	valid for $0.01 \le V_G \le 0.1$ m/s
Bando et al [44]	$k_L a_1 = 0.00062 D^{-0.5} V_G^{0.4} \mu_{eff}^{-1}$	(48a)	$8 \le (H_L/D) \le 13$, $0.1 \le D \le 0.5$ m, $0.01 \le V_G \le 0.08$ m/s, $0.73 \le n \le 0.85$
	$\frac{k_L a}{k_L a_1} - 1 = 2.2 e^{(-0.38 H_L/D)}$	(48b)	$1.3 \le (H_L/D) \le 8$ $0.1 \le D \le 0.5$ m, $0.01 \le V_G \le 0.08$ m/s, $0.73 \le n \le 0.85$

of the data sets is based on its linear transformation either from 0 to +1 or −1 to 1. However, the power function scaling or rather a nonlinear scaling approach is based on the exponential scaling followed by linear scaling of the input variables. GA is being used here to find the optimal values of exponents to the features for transformation in conjunction with SVR. The revised features are then considered for SVR-based modeling in order to establish correlations for overall gas hold-up, volumetric mass-transfer coefficient, and effective interfacial area for viscous media. The entire proposed approach is named as hybrid GA-SVR. For the purpose of establishing correlations, data sets for viscous media have been grouped as gas−(aqueous viscous Newtonian) and gas−(aqueous viscous non-Newtonian) systems. Results of hybrid GA-SVR model when compared with the conventional SVR model showed noticeable improvement in the prediction accuracies and reduction in error values.

The paper is organized as follows: existing literature and correlations on overall gas hold-up, volumetric mass-transfer coefficient, and effective interfacial area for viscous Newtonian and non-Newtonian liquid systems is discussed in section 2. Section 3 discusses the SVR-based modeling, followed by genetic algorithm and hybrid GA-SVR model in section 4. Eventually, section 5 compares and discusses about the results obtained through both the techniques.

2. Literature Review

2.1. Overall Gas Hold-up. 2.1.1. Viscous Newtonian Systems. To date, many researchers have carried out hydrodynamic studies in bubble column reactors and based on their experimental findings, the empirical correlations for overall gas hold-up have been proposed as listed in Table 1A. Akita and Yoshida[11] were the first to propose a dimensionless correlation. As can be seen from Table 1A, this correlation involves trial and error procedure for estimation of ϵ_G, thus making its usage very tedious when a large number of data points is involved. Besides, for viscous systems only three solutions of glycerol were considered while devising the correlation which severely limits its applicability for viscous liquids. On similar lines, Koide et al.[12] proposed an empirical correlation. This correlation, though valid for heterogeneous regime only, also involves trial and error procedure as was the case with eq 1 and is thus tedious to use. Bach and Pilhofer[13] proposed a correlation considering only buoyancy, inertial, and viscous forces. Here, the authors neglected surface tension force from their correlation, which has a major influence on ϵ_G. Also, the correlation, being valid only for pure liquids, cannot be used for solutions or mixtures. Hikita et al.[14] proposed an empirical correlation based on the experiments performed at ambient conditions using a single

Table 4. Range of Input and Output Parameters of SVR-Based Correlation for ϵ_G

parameters	viscous Newtonian systems	viscous non-Newtonian systems
range of output parameter, ϵ_G	0.001−0.628	0.006−0.36
	Operating Conditions	
pressure, kPa	100−1360	100−101.325
temperature, K	293−538	289−298
superficial gas velocity, m/s	0.00012−0.535	0.0028−0.288
superficial liquid velocity, m/s	0−0.00183	0−0.179
	Gas−Liquid Properties	
gas		
density, kg/m^3	0.166−11.32	1.18−1.22
molecular weight	4.0026−146.05	28.84
liquid		
density, kg/m^3	655−1380	991−1110
viscosity, Pa s	0.00055−0.55	0.0026−5.725
surface tension, N/m	0.0151−0.076	0.056−0.073
	Reactor Geometry	
column diameter, m	0.04−0.38	0.05−1
liquid height, m	0.2−3.6	0.2−5.75
sparger type	ring, single nozzle, multiple nozzle, perforated plate, sintered plate, spider, cross	ring, single nozzle, multiple nozzles, spider, perforated plate, sintered plate
sparger hole diameter, m	0.00003−0.01	0.0000175−0.013

Table 5. Range of Input and Output Parameters of SVR-Based Correlation for k_La

parameters	viscous Newtonian systems	viscous non-Newtonian systems
range of output parameter, k_La (1/s)	0.000116−0.264	0.00028−0.089
	Operating Conditions	
pressure, kPa	100−4240	100−101.325
temperature, K	293−364	292−301
superficial gas velocity, m/s	0.000242−0.408	0.002−0.423
superficial liquid velocity, m/s	0−0.0026	0−0.0224
	Gas−Liquid Properties	
gas		
density, kg/m^3	0.953−51.6	1.17−1.83
viscosity, Pa s	0.0000148−0.0000209	0.0000148−0.0000185
molecular weight	28.01−44	28.84−44
liquid		
density, kg/m^3	726−1264	991−1008.4
viscosity, Pa.s	0.0005−0.109	0.0019−1.91
surface tension, N/m	0.0164−0.0746	0.056−0.073
diffusivity of gas into liquid, m^2/s	$2.9 \times 10^{-11} - 3.26 \times 10^{-8}$	$1.26 \times 10^{-11} - 2.5 \times 10^{-9}$
	Reactor Geometry	
column diameter, m	0.04−0.38	0.1−0.6
liquid height, m	0.85−3.2	0.15−5.75
sparger type	ring, single nozzle, multiple nozzle, perforated plate, sintered plate, spider, cross	ring, single nozzle, multiple nozzles, spider, perforated plate, sintered plate
sparger hole diameter, m	0.00003−0.004	0.000017−0.013

nozzle sparger, which restricts its applicability to such kinds of spargers at ambient conditions only. Sotelo et al.[15] modified eq 3 and included a term (d_0) to account for sparger geometry. However, the effect of sparger geometry did not get fully included, as the number of holes (N_0), another parameter having a pronounced effect on ϵ_G, especially when operating in homogeneous regimes, was neglected. Also, the exponent on V_G is nearly 1, contradicting what other researchers have obtained for bubble columns operated in churn-turbulent regimes. Further, Godbole et al.[16] proposed an empirical correlation without taking into account ρ_L, σ_L, and ρ_G, which have a pronounced effect on ϵ_G and thus cannot be neglected. Joshi et al.[1] proposed an empirical correlation for large-diameter bubble columns ($D > 0.15$ m). However, the correlation can only be used for high superficial gas velocities ($V_G > 0.08$ m/s), thus limiting its applicability for the homogeneous regime. Anabtawi et al.[17] investigated the effect of liquid height on ϵ_G and proposed a correlation. However, ϵ_G was shown to vary directly as a function of σ_L, implying that ϵ_G increases with an increase in σ_L, which contradicts the work carried out by other authors. Also the parameters σ_L and ρ_L are investigated for a very narrow range, thus restricting its applicability. Urseanu et al.[18] proposed a correlation based on experiments carried out at high pressure (500, 800, and 1000 kPa). The authors did not find any dependence of σ_L and ρ_L on ϵ_G, although, with the liquids and operating conditions used, σ_L and ρ_L vary from 0.031 to 0.076 N/m and from 867 to 1380 kg/m^3, respectively, and hence have a pronounced effect on ϵ_G. Kazakis et al.[19] proposed a correlation incorporating d_0 in it. The authors obtained an exponent of 0.84 on D, thus indicating that ϵ_G increases almost linearly with D, which is contrary to what other researchers have investigated. Very recently the work of Nedeltchev and Schumpe[20] described gas hold-up as a function of bubble properties (bubble diameter, surface area, rise velocity, and frequency) with an additional term of bubble correction factor due to the difference in bubble shapes.

Apart from above-mentioned authors, experimental studies were carried out by Yoshida and Akita,[21] who evaluated

Table 6. Range of Input and Output Parameters of SVR-Based Correlation for $\underline{a}$

parameters	viscous non-Newtonian systems
range of output parameter $\underline{a}$, (1/m)	5.872−186.2
Operating Cconditions	
pressure, kPa	101.325
temperature, K	293−298
superficial gas velocity, m/s	0.0026−0.244
superficial liquid velocity, m/s	0−0.006
Gas−Liquid Properties	
gas	
density, kg/m^3	1.18−1.2
molecular weight	28.84
liquid	
density, kg/m^3	1091−1110
viscosity, Pa.s	0.0182−0.538
surface tension, N/m	0.0745−0.0755
Reactor Geometry	
column diameter, m	0.14−0.557
liquid height, m	1.88−2.5
sparger type	perforated plate
sparger hole diameter, m	0.0002−0.002

dependencies of liquid viscosity (μ_L), superficial gas velocity (V_G), column diameter (D), hole diameter (d_0), operating temperature (T), and liquid height (H_L) on ϵ_G, while Aoyama et al.[22] highlighted the effect of superficial liquid velocity (V_L) on ϵ_G. Zahradnik et al.[23] studied the effects of various liquid properties (ρ_L, σ_L, and μ_L) on ϵ_G, while Terasaka and Tsuge[24] varied d_0 and number of holes (N_0) to evaluate their dependencies on ϵ_G. Daly et al.[25] and Chabot and Lasa[26] through their experiments highlighted the effect of temperature on ϵ_G, while Soong et al.[27] investigated the effect of pressure on ϵ_G. Kuncova and Zahradnik[28] and Zahradnik et al.[29] studied the effect of liquid viscosity on ϵ_G. Macchi et al.[30] evaluated the effect of gas properties on ϵ_G by using various gases.

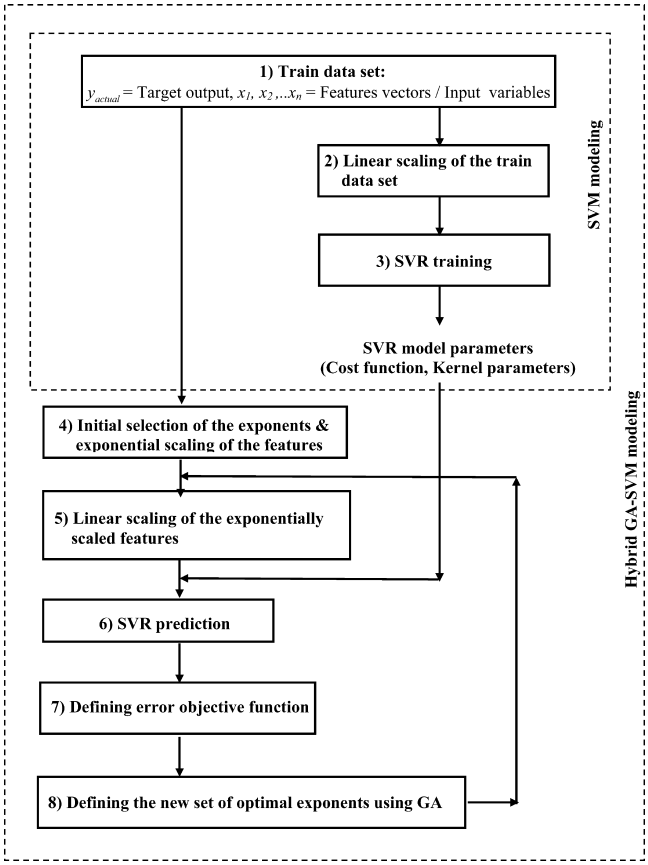

Figure 1. Flow chart of SVR and hybrid GA-SVR modeling approaches.

2.1.2. Viscous Non-Newtonian Systems. The correlations proposed for viscous non-Newtonian systems are listed in Table 1B. Godbole et al.[16] proposed two correlations based on their experimental measurements. Equation 11b includes the diameter effect but excludes the effect of liquid viscosity on ϵ_G. Godbole et al.[31] and Fransolet et al.[32] also proposed similar correlations. Lakota[33] proposed two empirical correlations based on experimental data. Equation 21a predicts a very weak dependence of μ_{eff} on ϵ_G, while other authors predict a strong influence on ϵ_G when viscous liquids are used. All of the above-mentioned correlations (eqs 11a, 11b, 13, 20, 21a, and 21b) neglect liquid properties (σ_L and ρ_L) as well as gas properties (ρ_G) which also have a pronounced effect on ϵ_G. Besides, these correlations were based on a very limited data set, thus limiting their applicability for large data sets.

Schumpe and Deckwer[34] and Devine et al.[35] have proposed empirical correlations valid for different flow regimes. However, they have neglected the effect of μ_{eff} in the proposed correlations (eqs 12a, 12b, and eq 14]. Kawase and Moo-Young[36] and Kawase et al.[37] proposed an empirical and a theoretical correlation, respectively. They carried out experiments in a bubble column where $H_L/D < 5$ was maintained. For such conditions, sparger geometry governs the flow patterns for the entire range of superficial gas velocities but the authors have neglected effects of sparger geometry in eq 16 and eq 17. The authors also neglect σ_L and ρ_G, while eq 17 fails to consider the effect of μ_{eff} on ϵ_G. Haque et al.,[38] on the baisis of experiments in large-diameter columns, proposed an empirical correlation. They investigated the effect of liquid height on ϵ_G but considered its effect on ϵ_G negligible while operating in the churn-turbulent regime. However, the correlation cannot be used for homogeneous regime, thus limiting its applicability. Vatai and Tekic,[39] on the basis of their experimental measurements with a single n,ozzle sparger, proposed two correlations in which constants of eqs 11b and 16 were modified. Equation 19a being valid for homogeneous regime, neglects sparger geometry, which governs the flow patterns in this regime, while eq 19b does not include μ_{eff}, which has a pronounced effect on ϵ_G especially when viscous media are used. In all of the correlations mentioned above for viscous non-Newtonian systems, σ_L which also has a pronounced effect on ϵ_G has been neglected. Schumpe and Deckwer[40] proposed an empirical correlation based on experiments carried out with aqueous solutions of carboxy methyl cellulose (CMC), sodium polyacrylamide (PAA), and xanthan. Their correlation though includes σ_L, it predicts an increase in ϵ_G with an increase in σ_L, which is contrary to what other researchers have obtained. Besides, gas properties have been neglected in all the correlations mentioned above for viscous non-Newtonian systems.

Apart from the above-mentioned authors, experimental studies were carried out by Buchholz et al.,[41] Deckwer et al.,[42] Haque et al.,[43] and Bando et al.[44] using air−(aqueous CMC solutions) to study hydrodynamics in bubble columns of varying dimensions. Popovic and Robinson[45] used air and aqueous solutions of CMC dissolved in 0.8 M Na_2SO_3 solution for their experiments, while Moo-Young and Kawase[46] studied hydrodynamics in a bubble column with $H_L/D < 5$ using viscoelastic aqueous Separan solutions, while Eickenbusch et al.[47] used large-diameter bubble columns to evaluate ϵ_G using air−(aqueous hydroxypropyl guar gum solutions).

Table 7. Optimal Values of the Exponents for the Individual Features Obtained through GA for Different Input Parameters

	parameter for given gas−liquid system				
	ϵ_G		$k_L\underline{a}$		$\underline{a}$
	gas−(aqueous viscous Newtonian solution)	gas−(aqueous viscous non-Newtonian solution)	gas−(aqueous viscous Newtonian solution)	gas−(aqueous viscous non-Newtonian solution)	gas−(aqueous viscous non-Newtonian solution)
a (V_G)	0.821	0.822	−0.042	0.095	0.0128
b (V_L)	0.272	1.613	0.542	0.528	0.582
c (k_d)	0.304	−0.827	0.706	0.705	0.812
d (d_0)	0.341	1.063	0.162	0.612	−1.770
e (N_0)	0.875	2.116	0.308	0.098	0.521
f (μ_L)	0.529	1.019	0.054	0.047	1.220
g (σ_L)	0.438	1.042	0.166	0.049	1.068
h (ρ_L)	0.370	0.087	0.541	0.161	0.052
i (D_L)			0.544	0.859	
j (μ_G)			1.435	0.614	
k (ρ_G)	0.717	−3.69	0.374	0.485	0.168
l (M_W)	0.804	1.638	−0.536	0.897	0.616
m (D)	0.458	0.915	0.408	0.260	0.106
n (H_L)	0.155	−0.246	1.628	0.974	0.504
o (P)	0.625	−0.221	1.233	−0.225	1.208
p (T)	0.655	−0.116	1.536	0.446	0.194

Table 8. Parameter Selection for Hybrid GA-SVR-Based Models for ϵ_G, $\underline{a}$, and $k_L\underline{a}$ for the Considered Gas−Liquid (Viscous Newtonian or Non-Newtonian) System

	ϵ_G[a]		$k_L\underline{a}$[b] (1/s)		$\underline{a}$[c] (1/m)
	viscous Newtonian	viscous non-Newtonian	viscous Newtonian	viscous non-Newtonian	viscous non-Newtonian
C	1.1	42	55	12	794
$\gamma = (1)/(2\sigma^2)$	15.7	30	1.16	1.64	1.6
ε	0.00001	0.00100	0.00110	0.00010	0.00015
no. of support vectors	1618	818	446	546	202
no. of training data points	1629	845	500	556	208
no. of Population ($N_{pop.}$)	20	20	20	20	20
crossover rate	0.8	0.8	0.8	0.8	0.8
mutation rate	0.2	0.2	0.2	0.2	0.2
no. of generations (N_{gen})	100	100	100	100	100

[a] Overall gas hold-up. [b] Volumetric mass-transfer coefficient. [c] Effective interfacial area.

Thus, from the above discussion, it is clear that none of the correlations for ϵ_G for both viscous Newtonian and non-Newtonian systems involve all the parameters signifying sparger effects and most of the correlations neglect gas properties. The effect of liquid flow rate on ϵ_G has also been neglected in all of the correlations mentioned above. In view of such a status of knowledge, it is the objective of this study to propose correlations for ϵ_G for viscous Newtonian and non-Newtonian systems. For this purpose, 14 parameters were selected which were superficial gas velocity (V_G), superficial liquid velocity (V_L), sparger type, sparger hole diameter (d_0), number of holes (N_0), liquid viscosity (μ_L), liquid surface tension (σ_L), liquid density (ρ_L), gas density (ρ_G), molecular weight of gas (M_W), column diameter (D), liquid height (H_L), operating pressure (P), and operating temperature (T). For viscous non-Newtonian liquids μ_L was replaced by μ_{eff} with the rest of the parameters remaining the same.

2.2. Effective Interfacial Area: Viscous Non-Newtonian Systems. Since no published information is available on viscous Newtonian systems, the present study considers the effect on effective interfacial area only for non-Newtonian systems. Schumpe and Deckwer,[34] Godbole et al.,[31] and Popovic and Robinson[48] carried out experiments for the measurement of $\underline{a}$ in bubble columns of different geometries using aqueous CMC solutions dissolved in 0.8 M Na_2SO_3 solutions. On the basis of their experimental results, empirical correlations were proposed which are summarized in Table 2. Equations 24 and 25 are based on experiments carried out in systems where the liquid phase is in batch mode, while eq 23 is obtained in systems where the liquid phase is in continuous mode. The authors have neglected the effect of liquid velocity in eq 23. Besides, all three correlations neglect σ_L, ρ_L, and ρ_G, which also have a pronounced effect on $\underline{a}$. Kawase et al.[37] made experimental measurements in a column having $H_L/D < 5$ to validate a theoretical correlation proposed by them. With $H_L/D < 5$, sparger geometry governs the bubble size and flow distribution patterns for the entire range of operation. The authors neglected parameters defining sparger geometry and found the effect of μ_{eff} on $\underline{a}$ negligible, while both these parameters have pronounced effect on $\underline{a}$.

Thus, it can be seen that, in all the correlations for $\underline{a}$, many important parameters such as sparger geometry, gas properties, and liquid flow rate have not been considered. In view of such a status of knowledge, it is the objective of this study to propose correlation for $\underline{a}$ for viscous non-Newtonian systems. For this purpose, 14 parameters were selected, which were superficial gas velocity (V_G), superficial liquid velocity (V_L), sparger type, sparger hole diameter (d_0), number of holes (N_0), liquid viscosity (μ_L), liquid surface tension (σ_L), liquid density (ρ_L), gas density (ρ_G), molecular weight of gas (M_W), column diameter (D), liquid height (H_L), operating pressure (P), and operating temperature (T).

2.3. Volumetric Mass-Transfer Coefficient. 2.3.1. Viscous Newtonian Systems. All the correlations proposed in the published literature to date are summarized in Table 3A. Akita and Yoshida[11] proposed a dimensionless correlation for $k_L\underline{a}$. The authors recommend the use of eq 1 for the estimation of ϵ_G, which, as has been mentioned above, is a tedious task involving trial and error procedure. The authors varied the temperature to study the effects of gas properties (ρ_G, μ_G) but

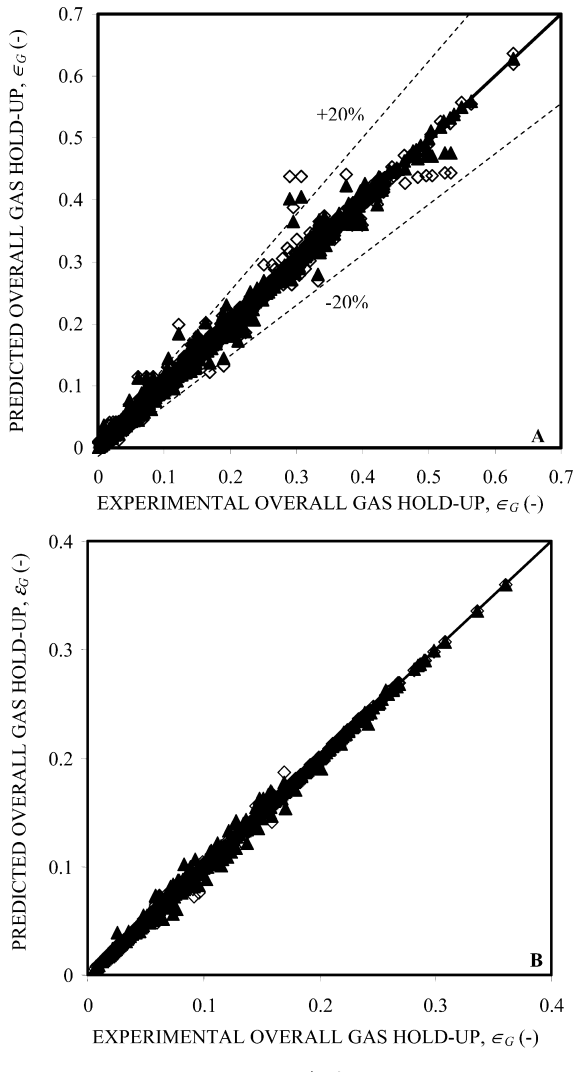

Figure 2. Parity plot for ϵ_G. (A) Viscous Newtonian system (training data): ◇, SVR; ▲, SVR-GA. (B) Viscous non-Newtonian system (training data): ◇, SVR; ▲, SVR-GA.

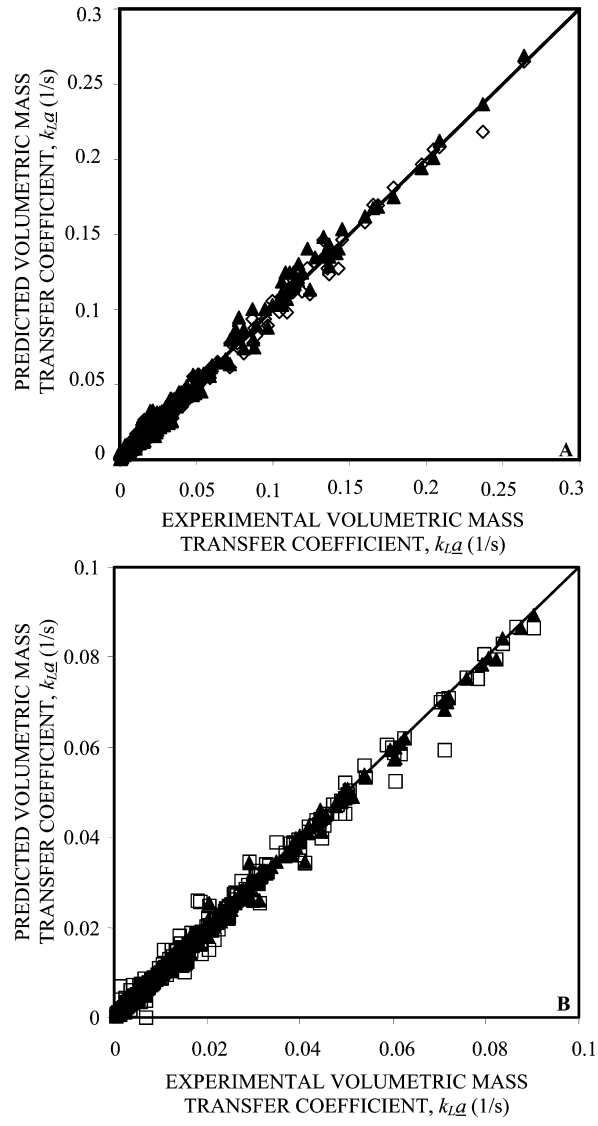

Figure 3. Parity plot for k_La. (A) Viscous Newtonian system (training data): ◇, SVR; ▲, SVR-GA. (B) Viscous non-Newtonian system (training data): □, SVR; ▲, SVR-GA.

have neglected their effects in eq 27. Nakanoh and Yoshida[49] in their empirical correlation show a linear dependency of V_G on k_La, which is contrary to what other researchers have obtained for the range of operation employed by them. Similar to eq 28, Schumpe and Deckwer[40] proposed an empirical correlation. Here, too, the authors have neglected the effect of varying gas properties (ρ_G and μ_G) in their correlation. Besides it, eqs 28 and 32 have been obtained for data sets at ambient conditions and, hence, cannot be used for high-temperature and high-pressure applications. Terasaka and Tsuge[24] included N_0 in their dimensionless correlation to quantify the effect of the number of holes on k_La with the rest of the parameters remaining similar to eq 28. Equation 35 is applicable only when multiple nozzles are used which fall within the range for N_0 as specified in Table 3A. These experiments were carried out for the range $0.000242 < V_G < 0.0182$ m/s, suggesting that the regime of operation was homogeneous. Thus, d_0 and also N_0 play an important role in determining k_La for the operating conditions used; still the effect of N_0 was neglected in their correlation. The range investigated is also very small, thus further limiting its applicability.

Hikita et al.[50] included μ_G in their correlation as they carried out experiments with various gases but did not include the effect of ρ_G on k_La. A single nozzle was used as sparger, while V_G was varied from 0.042 to 0.38 m/s, indicating that both homogeneous and heterogeneous regimes were covered. However, the effects of sparger geometry were neglected from their correlation. Sotelo et al.[15] modified eq 32 and included d_0 in their correlation to account for sparger geometry. They varied V_G from 0.00645 to 0.0066 m/s, indicating that the regime of operation was mostly homogeneous. But like eq 35 only d_0 was considered while N_0 was excluded. Besides it, eq 36 can be used only for porous plates and for the range mentioned in Table 3A, thus limiting its applicability. Koide et al.[12] investigated the effect of d_0 and N_0 on k_La but considered their effects negligible and, hence, excluded these parameters from their correlation. The range for which eq 30 is valid is very small, while effects of D, ρ_G, and μ_G on k_La have also been neglected. Kawase and Moo-Young[36] and Kawase et al.[37] proposed an empirical and a theoretical correlation, respectively. Both correlations were developed for systems having $H_L/D < 5$. For such conditions, sparger design governs the flow patterns and, hence, the mass-transfer rates. However, the authors did not include the role of sparger design in their correlations. Besides it, σ_L has also been neglected in eq 31. Ozturk et al.[51] used d_B as the characteristic dimension instead of D in their correlation. They suggested the use of $d_B = 0.003$ m for all the liquids studied by them on the basis of experiments carried out by

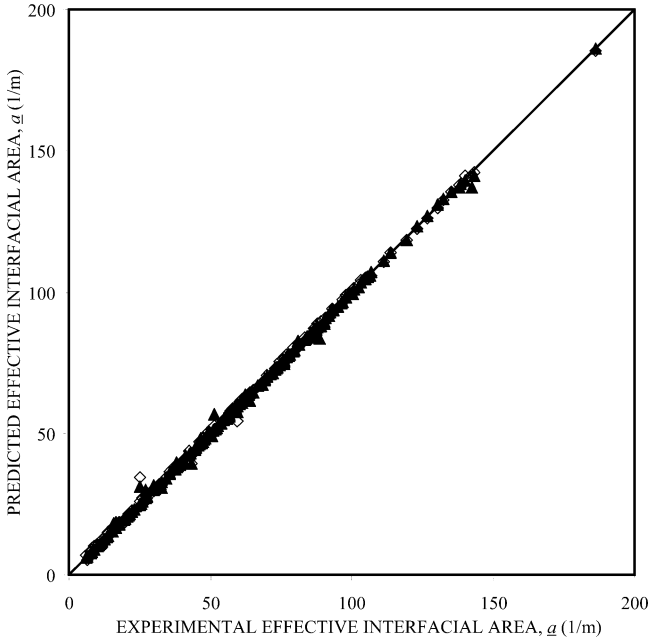

Figure 4. Parity plot for viscous non-Newtonian system for $\underline{a}$ (training data): ◇, SVR; ▲, SVR-GA.

Quicker and Deckwer[52] for liquids such as xylene, decalin, and *n*-paraffin for a temperature range of 333−443 K; however, this may not be true for viscous liquids as their characteristics are very different from the liquids mentioned above. Use of d_B in eq 34 requires estimation from experiments, which is very difficult and, hence, unsuitable for use. Alvarez et al.[53] included a constant term in their correlation for quantifying the use of porous spargers in the experiments. Thus, correlation's validity is restricted only for porous plates for the narrow range for d_0 mentioned in Table 3A. Lau et al.[54] proposed an empirical correlation based on experiments at varying pressures (100−4240 kPa) and varying temperatures (298−365 K) excluding the effects of μ_G, ρ_G, and D_L although at the operating conditions used, these parameters have a pronounced effect on $k_L\underline{a}$. Very recently the work of Nedeltchev et al.[55] describes $k_L\underline{a}$ as function of bubble properties (bubble diameter, surface area, rise velocity, and frequency) with an additional term of bubble correction factor due to difference in bubble shapes.

Apart from the above-mentioned authors, experimental studies were carried out by Yoshida and Akita,[21] Merchuk and Ben-Zvi,[56] Vandu and Krishna,[57] and Fujie et al.,[58] wherein they evaluated dependencies of liquid properties (μ_L, σ_L, ρ_L, and D_L), superficial V_G, D, and d_0 on $k_L\underline{a}$.

2.3.2. Viscous Non-Newtonian Systems. All the proposed correlations for $k_L\underline{a}$ in non-Newtonian systems are summarized in Table 3B. Nakanoh and Yoshida[49] were the first to propose an empirical correlation for $k_L\underline{a}$ in non-Newtonian systems. The authors used Deborah number (*De*) which is the ratio of the relaxation (characteristic material) time to characteristic process

Table 11. Performance Indicators for Previous Literature Correlations, SVR-Based and SVR-GA-Based Correlations for Viscous Non-Newtonian Systems for $\underline{a}$

correlation	CC	AARE (%)
Schumpe and Deckwer[34]	0.95	99.00
Godbole et al.[31]	0.93	97.27
Popovic and Robinson[48]	0.89	27.40
Kawase et al.[37]	0.82	56.05
SVR (this work)	0.99	2.19
GA-SVR (this work)	0.99	1

Table 9. Performance Indicators for Previous Literature Correlations, SVR-Based and SVR-GA-Based Correlations for Viscous Newtonian and Non-Newtonian Systems for ϵ_G

viscous Newtonian systems			viscous non-Newtonian systems		
correlation	CC	AARE (%)	correlation	CC	AARE (%)
Akita and Yoshida[11]	0.68	43.50	Godbole et al.[16]	0.815	29.40
Bach and Pilhofer[13]	0.71	207.28	Schumpe and Deckwer[34]	0.674	40.82
Hikita et al.[14]	0.50	37.29	Godbole et al.[31]	0.424	36.70
Godbole et al.[16]	0.73	0.41	Devine et al.[35]	0.995	10.62
Sotelo et al.[15]	0.58	218.41	Kawase and Moo-Young[36]	0.843	21.43
Joshi et al.[1]	0.69	29.52	Haque et al.[38]	0.862	14.91
Anabtawi et al.[17]	0.99	46.34	Kawase et al.[37]	0.796	22.77
Urseanu et al.[18]	0.74	41.18	Schumpe and Deckwer[40]	0.86	19.50
Kazakis et al.[19]	0.35	329.50	Vatai and Tekic[39]	0.645	46.70
SVR (this work)	0.99	12.33	Fransolet et al.[32]	0.729	30.83
GA-SVR (this work)	0.99	3.75	Lakota[33]	0.802	56.57
			Lakota[33]	0.779	33.60
			SVR (this work)	0.999	1.85
			GA-SVR (this work)	0.999	1.65

Table 10. Performance Indicators for Previous Literature Correlations, SVR-Based and SVR-GA-Based Correlations for Viscous Newtonian and Non-Newtonian Systems for $k_L\underline{a}$

viscous Newtonian systems			viscous non-Newtonian systems		
correlation	CC	AARE (%)	correlation	CC	AARE (%)
Akita and Yoshida[11]	0.34	76.37	Deckwer et al.[42]	0.07	131.98
Nakanoh and Yoshida[49]	0.66	134.18	Godbole et al.[31]	0.72	48.69
Hikita et al.[50]	0.85	46.53	Kawase and Moo-Young[36]	0.16	122.91
Koide et al.[12]	0.43	131.50	Kawase et al.[37]	0.14	138.76
Kawase and Moo-Young[36]	0.55	45.68	Schumpe and Deckwer[40]	0.86	33.69
Schumpe and Deckwer[40]	0.63	88.65	Popovic and Robinson[48]	0.19	39.38
Kawase et al.[37]	0.63	66.76	Vatai and Tekic[39]	0.004	99.98
Ozturk et al.[51]	0.84	37.84	Merchuk and Ben-Zvi[56]	0.15	192.15
Sotelo et al.[15]	0.57	584.87	Bando et al.,[44] eq 48a	0.95	51.28
Lau et al.[54]	0.67	869.75	Bando et al.,[44] eq 48b	0.75	50.85
SVR (this work)	0.99	18.35	SVR (this work)	0.99	9.74
GA-SVR (this work)	0.98	8.60	GA-SVR (this work)	0.99	1.91

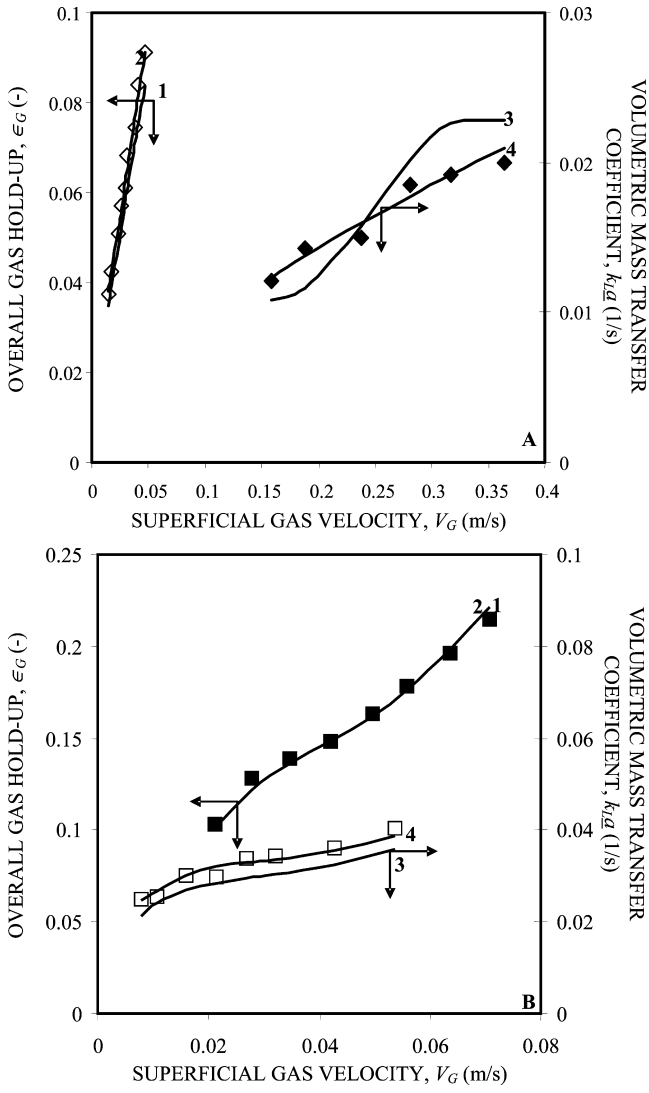

Figure 5. (A) Comparison of SVR prediction with the experimental data of various authors for viscous Newtonian systems: ◇, experimental data of De Swart and Krishna[65] for ϵ_G vs —, 1 (SVR) and 2 (SVR-GA); ♦, experimental data of Vandu and Krishna[57] for $k_L\underline{a}$ vs —, 3 (SVR) and 4 (SVR-GA). (B) Comparison of SVR prediction with the experimental data of various authors for viscous non-Newtonian systems: ●, experimental data of Vatai and Tekic[39] for ϵ_G vs —, 1 (SVR) and 2 (SVR-GA); □, experimental data of Buchholz et al.[41] for $k_L\underline{a}$ vs —, 3 (SVR) and 4 (SVR-GA).

time to account for the viscoelastic nature of aqueous PAA solutions. This parameter requires the knowledge of bubble diameter, bubble rise velocity, and characteristic material time. The knowledge of these parameters can be obtained only by doing experiments thus making eq 39 unsuitable for use. Also, the authors predict a linear dependency of V_G on $k_L\underline{a}$, which is contrary to what other researchers have obtained. Schumpe and Deckwer[40] based on their experiments with aqueous CMC, xanthan, and PAA solutions proposed an identical correlation as eq 39 but without *De* in it. The authors discovered that eq 44 failed for aqueous PAA solutions due to their viscoelastic nature, thus making it unsuitable for viscoelastic fluids. Vatai and Tekic[39] used the same dimensionless parameters as that in eq 39 but without considering *De* and *Ga* in the correlation. It predicts a linear dependency of V_G on $k_L\underline{a}$, which contradicts what other researchers have obtained. Also, eq 46 fails for viscoelastic PAA solutions. Suh et al.[59] in their correlation used the Weissenberg number (*Wi*), which is the ratio of first normal stress difference to shear rate to account for the viscoelastic behavior of PAA solutions. Equation 47 as such has

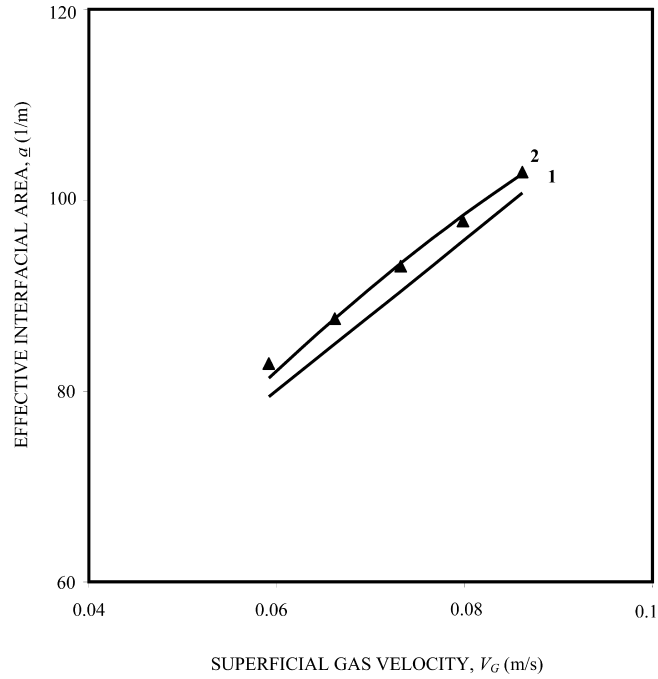

Figure 6. Comparison of SVR prediction with the experimental data for viscous non-Newtonian systems for $\underline{a}$: ▲, experimental data of Schumpe and Deckwer[34] vs —, 1 (SVR) snf 2 (SVR-GA).

practical usage only for systems for which *Wi* has been experimentally derived. Thus, it can be used for data sets obtained by the authors in their experiments only. The authors have derived eq 47 for heterogeneous and slug flow regimes only and, hence, cannot be used for homogeneous regime.

Deckwer et al.[42] proposed an empirical correlation for slug flow regime, while Godbole et al.[31] proposed a similar correlation for churn-turbulent regime. The range for eq 40 is very narrow as the flow behavior index (n) varies from 0.82 to 0.92. In eq 40 and eq 41, liquid properties (σ_L and ρ_L) and gas properties (ρ_G, μ_G, and D_L) have been neglected although the literature shows that all these factors affect $k_L\underline{a}$. Kawase and Moo-Young[36] and Kawase et al.[37] proposed an empirical and a theoretical correlation, respectively. They carried out their experiments in bubble columns where $H_L/D < 5$ was maintained. Sparger geometry which plays a major role in defining mass-transfer rates when $H_L/D < 5$ is maintained has also been neglected in the correlation. Gas properties (ρ_G, μ_G) have also been neglected, while eq 42, besides neglecting the above-mentioned parameters, also neglects surface tension (σ_L). Popovic and Robinson[45] proposed an empirical correlation after carrying out regression analysis of their experimental data. Here, although the authors have evaluated the effect of liquid velocity on $k_L\underline{a}$, they neglected its effect on $k_L\underline{a}$ in eq 45. The authors also predict a linear dependency of ρ_L on $k_L\underline{a}$, which contradicts what other researchers have obtained. Merchuk and Ben-Zvi[56] proposed a correlation based on shear rates wherein shear rate was defined as a function of V_G, k, n, H_L, $\underline{a}$, and pressures at the top and bottom of the column. For estimation of $\underline{a}$, the authors recommend use of eq 23. Equations 48 although valid for homogeneous and churn-turbulent regimes is based on a limited data set and, hence, cannot be used as a generalized correlation. Besides, no consideration has been given to liquid properties (σ_L and ρ_L), gas properties (ρ_G, μ_G, and D_L) as also sparger geometry, which in the present case plays a major role in governing mass-transfer rates as the regimes of operation are homogeneous and churn-turbulent. Bando et al.[44] included a parameter quantifying the effect of liquid heights on $k_L\underline{a}$ in their correlations. The investigated range is very small, indicating that very few liquids have been used in deriving their

Table 12. Simulation Conditions and Results of SVR- and SVR-GA-Based Models for the Test Data Sets for ϵ_G, $k_L\underline{a}$, and $\underline{a}$

	parameter for the given gas−liquid system				
	ϵ_G		$k_L\underline{a}$		$\underline{a}$
	gas−(aqueous viscous Newtonian solution) (air−(paraffin oil)); De Swart and Krishna[65]	gas−(aqueous viscous non-Newtonian solution) (air−(aqueous CMC solution)); Vatai and Tekic[39]	gas−(aqueous viscous Newtonian solution) (air−(tellus oil)); Vandu and Krishna[57]	gas−(aqueous viscous non-Newtonian solution) (air−(aqueous CMC solution)); Buchholz et al.[41]	gas−(aqueous viscous non-Newtonian solution) (air−(aqueous CMC/0.8 M Na_2SO_3 solution)); Schumpe and Deckwer[34]
superficial gas velocity (m/s)	0.15−0.04	0.02−0.07	0.15−0.36	0.007−0.05	0.05−0.08
superficial liquid velocity (m/s)	0	0	0	0.01	0.006
sparger type	perforated plate	single nozzle	perforated plate	sintered plate	perforated plate
sparger hole diameter (m)	0.0005	0.004	0.0005	0.00001	0.001
no. of sparger holes	2750	1	199	470204	73
liquid viscosity (Pa s)	0.075	0.029−0.034	0.075	0.059−0.85	0.02−0.021
liquid surface tension (N/m)	0.028	0.067	0.028	0.0696	0.0747
liquid density (kg/m^3)	862	1012	862	1006	1091
diffusivity of gas into liquid (m^2/s)			1.02×10^{-9}	2.058×10^{-9}	
gas viscosity (Pa s)			1.79×10^{-5}	1.82×10^{-5}	
gas density (kg/m^3)	1.2	1.18	1.2	1.18	1.18
molecular weight of gas	28.84	28.84	28.84	28.84	28.84
column diameter (m)	0.38	0.05	0.1	0.14	0.14
liquid height (m)	3.2	2	3.2	3.13	2.16
pressure (kPa)	101.32	101.32	101.32	101.32	101.32
temperature (K)	293	298	293	298	298
SVR (CC)	0.98	0.99	0.95	0.96	0.99
SVR (AARE %)	7.41	1.89	12.64	10.26	2.85
GA-SVR (CC)	0.98	0.99	0.95	0.96	0.99
GA-SVR (AARE %)	2.35	0.89	3.55	2.99	0.60

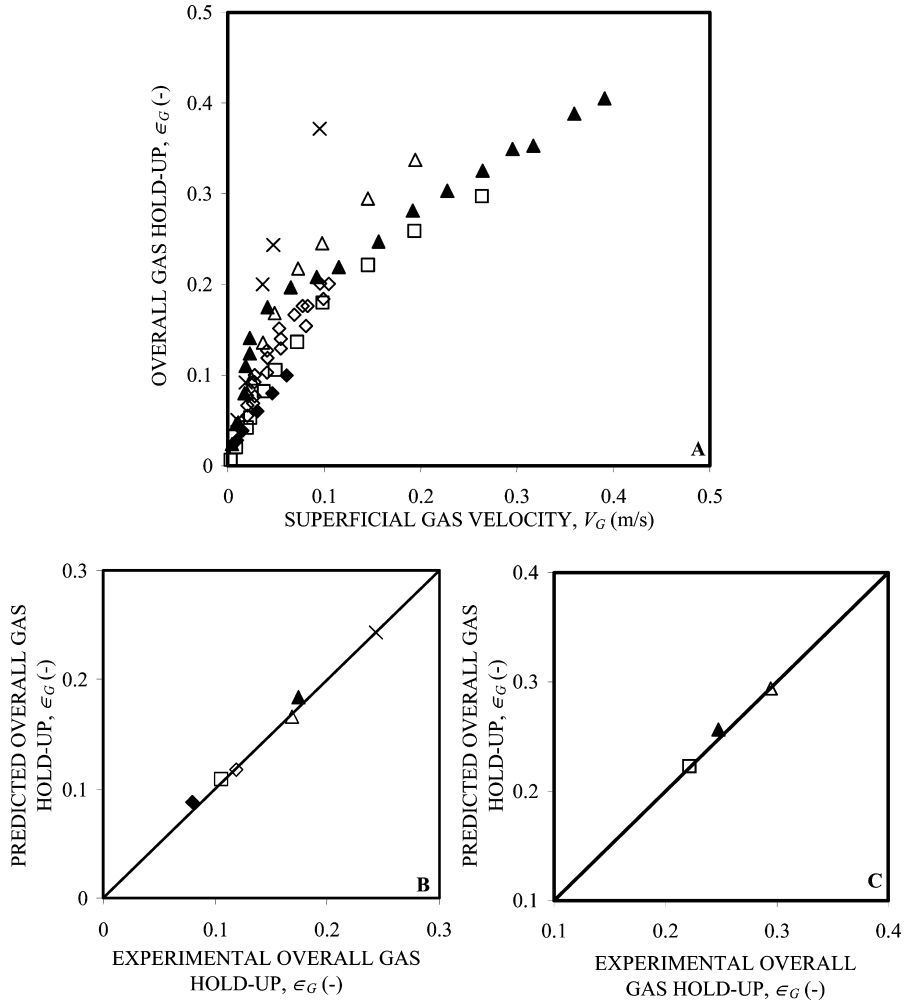

Figure 7. (A) ϵ_G values for viscous Newtonian systems, experimental data of Yoshida and Akita[21] (◇, air−(aqueous glycerol solution)), Macchi et al.[30] (□, helium−(aqueous glycerol solution); Δ, CO_2−(aqueous glycerol solution); ×, SF_6−(aqueous glycerol solution)), Vandu and Krishna[57] (▲, air−tetradecane), and Kuncova and Zahradnik[28] (◆, air−(aqueous sucrose solution). (B) Parity plot for $V_G = 0.045$ m/s using SVR. (C) Parity plot for $V_G = 0.145$ m/s using SVR.

correlation. Also, no consideration has been given to σ_L and ρ_L and gas properties ρ_G, μ_G, and D_L.

Apart from investigators mentioned above, experimental studies were carried out by Buchholz et al.[41] using air−aqueous CMC solutions, by Moo-Young and Kawase[46] using CO_2−aqueous Separan solutions, by Moo-Young and Kawase[60] using air−aqueous Carbopol solutions, and by Eickenbusch et al.[47] using air−aqueous solutions of hydroxypropyl guar gum. Thus, it can be seen that in all the correlations for $k_L\underline{a}$, many important parameters such as sparger geometry, gas properties, and liquid flow rate have not been considered or have not been quantified properly. In view of such a status of knowledge, it is the objective of this study to propose correlation for $k_L\underline{a}$ for viscous Newtonian and non-Newtonian systems. For this purpose, 16 parameters were selected which were V_G, V_L, sparger type, d_0, N_0, μ_L, σ_L, ρ_L, D_L, M_W, ρ_G, D, H_L, P, and T. For viscous non-Newtonian solutions, μ_L was replaced by μ_{eff}.

3. SVR-Based Modeling: Mathematical Modeling

The support vector regression (SVR) is an adaptation of a recently introduced statistical/machine learning theory known as, *support vector machines*.[61] The objective is to build an ε-SVR model[61] to fit a regression function, $y = f(x)$, such that it accurately predicts the outputs $\{y_i\}$ corresponding to a new set of input examples, $\{x_i\}$. To obtain the correct fit, SVR considers the following linear estimation function in the high dimensional feature space,[62]

$$f(x, w) = (w \cdot \phi(x) + b) \tag{49}$$

where $\phi(x)$ = function termed *feature* and $(w \cdot \phi(x))$ is the dot product in the feature space, F, such that $\phi(x) \rightarrow F$ and $w \in F$. Thus, after algebraic transformation, the objective function (eq 49) gets converted to convex optimization problem whose primal form is given as

$$\max\left(L(\alpha_{i,j}^*) = \sum_{i=1}^{N} y_i(\alpha_i - \alpha_i^*) - \varepsilon \sum_{i=1}^{N}(\alpha_i + \alpha_i^*)\right) - \frac{1}{2}\sum_{i=1}^{N}\sum_{j=1}^{N}(\alpha_i - \alpha_i^*)(\alpha_j - \alpha_j^*)(\phi(x_i)\cdot\phi(x_j)) \tag{50}$$

subject to constraints

$$C \geq \alpha_i, \quad \alpha_i^* \geq 0, \quad \text{and} \quad \sum_{i=1}^{N}(\alpha_i - \alpha_i^*)y_i = 0$$

where C is the cost function employed to obtain a trade-off between the *flatness* of the regression function and the amount to which deviations larger than ε (loss function) can be tolerated. Solution of eq 50 by convex quadratic programming (QP) gives the value of the coefficients α_i and α_i^*. Due to the specific character of the above-described quadratic programming prob-

lem, only some of the coefficients ($\alpha_i - \alpha_i^*$) are nonzero, and the corresponding input vectors, x_i, are called support vectors. These SVs are known as the most informative data points that compress the information content of the training set, thereby representing the entire SVR function. Thus, they are a subset of the input data set. These SVs, x_i, and the corresponding nonzero Lagrange multipliers α_i and α_i^* give the value of weight vector, w, followed by the expanded form of the SVR,

$$w = \sum_{i=1}^{N} (\alpha_i - \alpha_i^*)\phi(x_i) \tag{51}$$

$$f(x, \alpha_i, \alpha_i^*) = \sum_{i=1}^{N_{sv}} (\alpha_i - \alpha_i^*)(\phi(x_i)\cdot\phi(x_j)) + b \tag{52}$$

However, as can be seen from eq 50 with an increase in the input dimensions, the dimensions in the high dimensional feature space further increases by many folds, and thus eq 50 becomes computationally intractable. Such a problem can be overcome by defining appropriate kernel functions in place of the dot product of the input vectors in high dimensional feature space.

$$K(x_i, x_j) = (\phi(x_i)\cdot\phi(x_j)) \tag{53}$$

The advantage of a kernel function is that the dot product in the feature space can now be computed without actually mapping x_i into high dimensional feature space, thus allowing calculations to be done in the input space itself. Thus, the dual optimization problem (eq 50) gets revised to the following form:

$$\max(L(\alpha_{i,j}^*)) = \sum_{i=1}^{N} y_i(\alpha_i - \alpha_i^*) - \varepsilon \sum_{i=1}^{N} (\alpha_i + \alpha_i^*) - \frac{1}{2}\sum_{i=1}^{N}\sum_{j=1}^{N} (\alpha_i - \alpha_i^*)(\alpha_j - \alpha_i^*)K(x_i, x_j) \tag{54}$$

subject to constraints

$$C \geq \alpha_i, \quad \alpha_i^* \geq 0, \quad \text{and} \quad \sum_{i=1}^{N} (\alpha_i - \alpha_i^*)y_i = 0$$

Thus, the basic SVR formulation takes the following form:

$$f(x, \alpha_i, \alpha_i^*) = \sum_{i=1}^{N_{sv}} (\alpha_i - \alpha_i^*)K(x_i, x_j) + b \tag{55}$$

There exist several choices of kernel function K such as linear, polynomial, and Gaussian radial basis function. The most commonly used kernel function is the Gaussian radial basis function (RBF).[61] It is defined as

$$K(x_i, x_j) = \exp\left(\frac{-\|x_i - x_j\|^2}{2\sigma^2}\right) \tag{56}$$

where σ denotes the width of the RBF.

Further details regarding the SVR-based function can be obtained from Gandhi et al.[5]

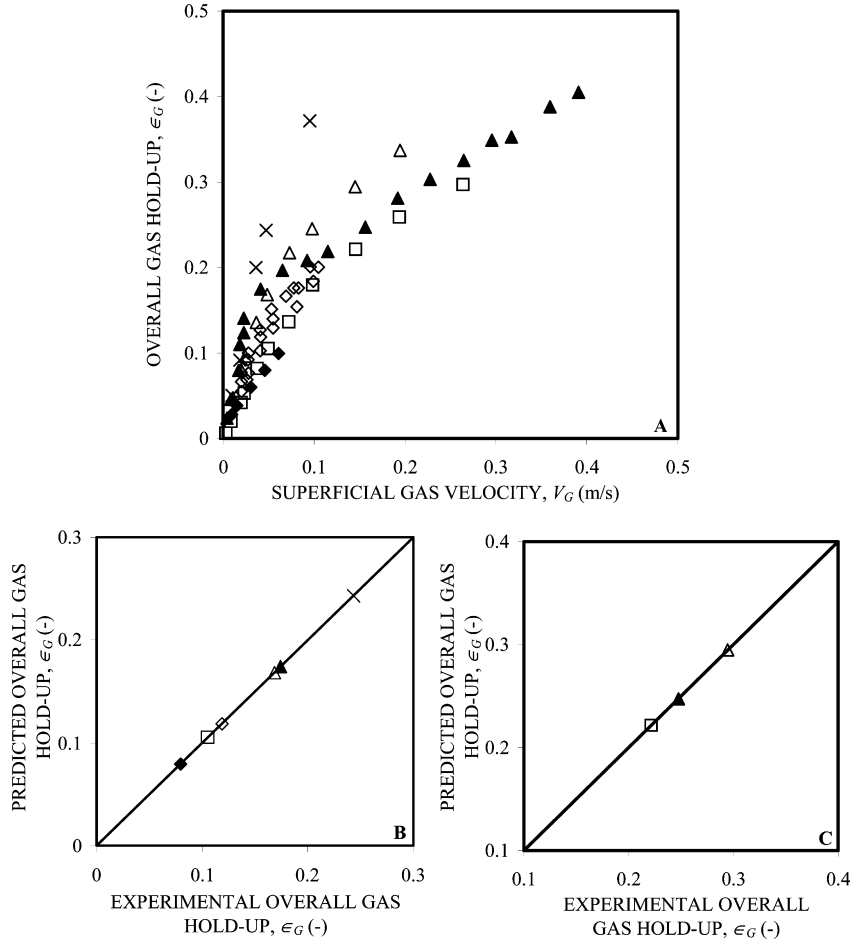

Figure 8. (A) ϵ_G values for viscous Newtonian systems, experimental data of Yoshida and Akita[21] (◇, air−(aqueous glycerol solution)), Macchi et al.[30] (□, helium−(aqueous glycerol solution); Δ, CO_2−(aqueous glycerol solution); ×, SF_6−(aqueous glycerol solution)), Vandu and Krishna[57] (▲, air−tetradecane), and Kuncova and Zahradnik[28] (◆, air−(aqueous sucrose solution). (B) Parity plot for $V_G = 0.045$ m/s using SVR-GA. (C) Parity plot for $V_G = 0.145$ m/s using SVR-GA.

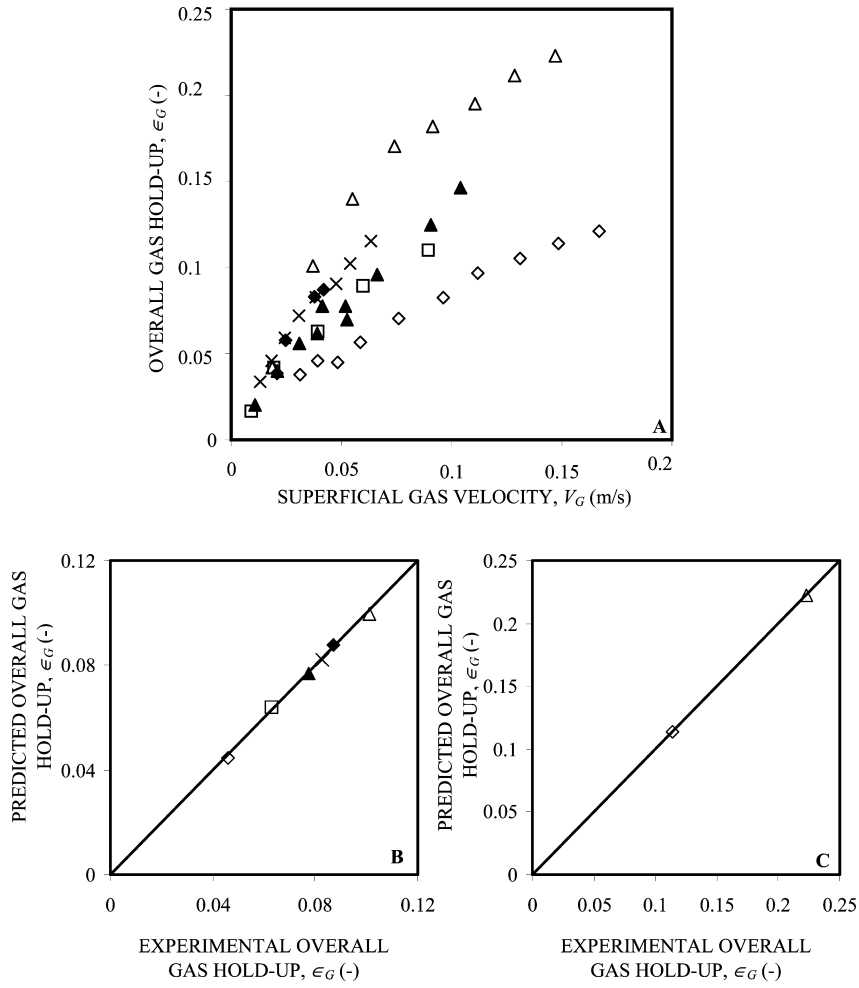

Figure 9. (A) $\epsilon_G$values for viscous non-Newtonian systems, experimental data of Deckwer et al.[42] (◆, air−(aqueous CMC solution)), Eickenbusch et al.[47] (□, air−(aqueous hydroxypropyl guar gum solution)), Fransolet et al.[32] (Δ, air−(aqueous xanthan solution)), Haque et al.[43] (◇, air−(aqueous CMC solution)), Kawase et al.[37] (×, air−(aqueous Carbopol solution)), and Popovic and Robinson [45](▲, air−(aqueous CMC dissolved in 0.8 M Na_2SO_3 solution). (B) Parity plot for $V_G = 0.041$ m/s using SVR. (C) Parity plot for $V_G = 0.145$ m/s using SVR.

4. Hybrid GA-SVR Model

4.1. Genetic Algorithm. Genetic algorithm (GA), an evolutionary algorithm is utilized to perform the optimization. GA is a conceptually simple and easy-to-program global optimization technique.[63] It is a facilitated random/stochastic search technique, well-known for its robustness, which exploits the supposed understanding of the genetic evolution phenomena to find an optimal solution of a given problem. The algorithm starts with a set of random solutions called population ($N_{pop.}$). Of these random solutions, an individual solution is represented in encoded form and is called a chromosome. Each chromosome comprises a sequence of individual structures called genes which represent the actual parameters to be optimized. The solutions from one population are used to generate the next population. To create a new population to certain probabilities, GA uses genetic operators, i.e., crossover (P_{cross}) and mutation (P_{mut}) and a selection process. These genetic operators are used to generate the new solutions (children population or offspring) from the current set of solutions (parent population), thereby driving the solution downhill toward the optimal solution, and also introduces globality into the solution. Selection reflects the principle of "survival of the fittest" and is the driving mechanism of keeping and deleting some solutions from the parent population to generate an offspring with the same number of chromosomes. During this selection process, the solutions are selected according to their values of objective function (usually referred to as fitness). A high fitness value of a chromosome corresponds to a higher chance to be selected for the next generation. The GA will repeat this process until a termination condition is satisfied either by choosing fixed number of generations (N_{gen}) or the best solution is returned (convergence) to represent the optimum solution. The procedure of GA can be summarized in the following steps:

(1) Choose a randomly generated population: For the present study, $N_{pop.}$ of 20 genes has been selected with all the exponents uniformly generated in the range of 0−1.

(2) Calculate the fitness of each chromosome in the population: For each gene a fitness score is calculated as the persent average absolute relative error (% AARE) on the validation set by SVR model generated using transformed variables. The parameters for SVR are kept the same as those used in the ecase of the model without variable transformation.

(3) Create the offspring by the genetic operators (selection, crossover, and mutation): All genes are then ranked according to the error, and mutation, selection, and crossover functions are applied. This results in formation of a new set of genes which have better scores that is lower errors than earlier generation.

(4) Check the termination condition: If the new population does not satisfy the termination condition, repeat steps 2 up to 4 for the generated offspring as a new starting population. Detailed theory and math of GA can be found in Goldberg[63] and Nandi et al.[9]

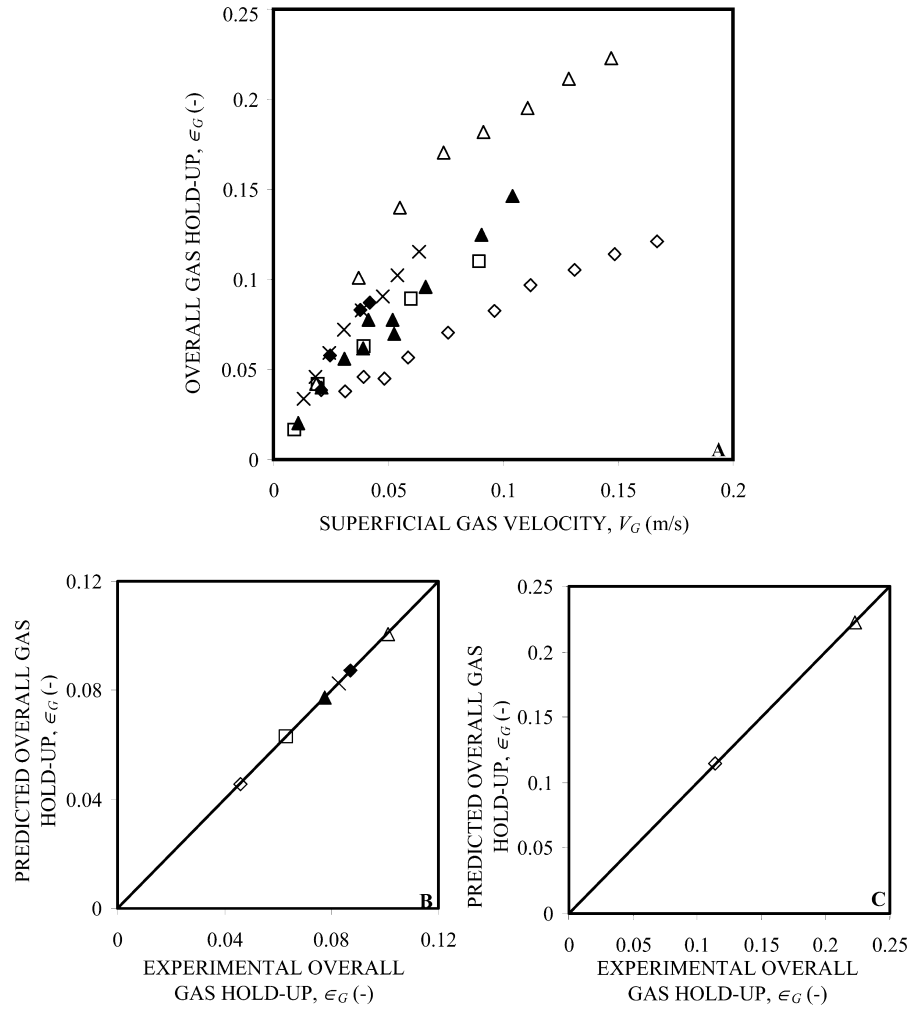

Figure 10. (A) ϵ_G values for viscous non-Newtonian systems, experimental data of Deckwer et al.[42] (◆, air−(aqueous CMC solution)), Eickenbusch et al.[47] (□, air−(aqueous hydroxypropyl guar gum solution)), Fransolet et al.[32] (Δ, air−aqueous xanthan solution), Haque et al.[43] (◇, air−(aqueous CMC solution)), Kawase et al.[37] (×, air−(aqueous Carbopol solution)), and Popovic and Robinson[45] (▲, air−(aqueous CMC dissolved in 0.8 M Na_2SO_3 solution)). (B) Parity plot for $V_G = 0.041$ m/s using SVR-GA. (C) Parity plot for $V_G = 0.145$ m/s using SVR-GA.

4.2. Hybrid GA-SVR Algorithm. The present study involves the use of power operation (exponents) for the scaling of the input variables/features.

$$y_{\text{pred}} = f(x_1^a, x_2^b, ..., x_n^n) \tag{57}$$

Thus, in short, the feature data set is subjected to exponential scaling prior to its transformation into high dimensional feature space (as a part of SVR training). GA has been used here to find the optimal values of these exponents for the attributes by minimizing the error between predicted and the actual target output values given as

$$\min[f(y_{\text{actual}} - y_{\text{pred}})] \tag{58}$$

The approach for finding the optimal values of exponents using GA has been carried out in conjunction with SVR modeling.

5. Establishment of SVR/GA-SVR-Based Correlations

5.1. Collection of Data Sets. For the purpose of establishing data driven based correlations it was thought desirable to build comprehensive data sets covering all the experimental studies published in the open literature. For this purpose, an extensive literature survey was done. Accordingly, data set was extracted from published literature by using software WINDIG 2.5. Thus, for ϵ_G, 1629 data points for viscous Newtonian and 845 data points for viscous non-Newtonian systems were collected, while, for $k_L\underline{a}$, 500 data points for viscous Newtonian and 556 data points for viscous non-Newtonian systems were collected. For $\underline{a}$, 208 data points for non-Newtonian systems only were collected as there is no published literature for viscous Newtonian systems. These data sets were collected from literature spanning the years 1965−2007. The range for the data set collected is shown in Tables 4−6 for ϵ_G, $k_L\underline{a}$, and $\underline{a}$, respectively.

5.2. Procedure for Estimating Regression Function. 5.2.1. SVR Model. In the present study, a SVR implementation known as ε-SVR in the LIBSVM software library[64] has been used to develop the SVR-based model for ϵ_G, $k_L\underline{a}$, and $\underline{a}$, respectively. The algorithm (Figure 1) for pursuing the same is detailed and numbered as follows:

(1) *Train data set*: Data set required for supervised training is collected as mentioned in section 5.1.

(2) *Scaling the train data set*: Entire data set (features/input variables and target outputs) is scaled between +1 and −1 in order to suppress the effect of the wide variation existing between the values of the input variables.

(3) *SVR training*: The scaled data set is subjected to SVR training for obtaining the optimal values of the model parameters (cost function and kernel parameters). The optimal values of these parameters are obtained using the cross-validation methodology. Detailed procedure for estimating regression function

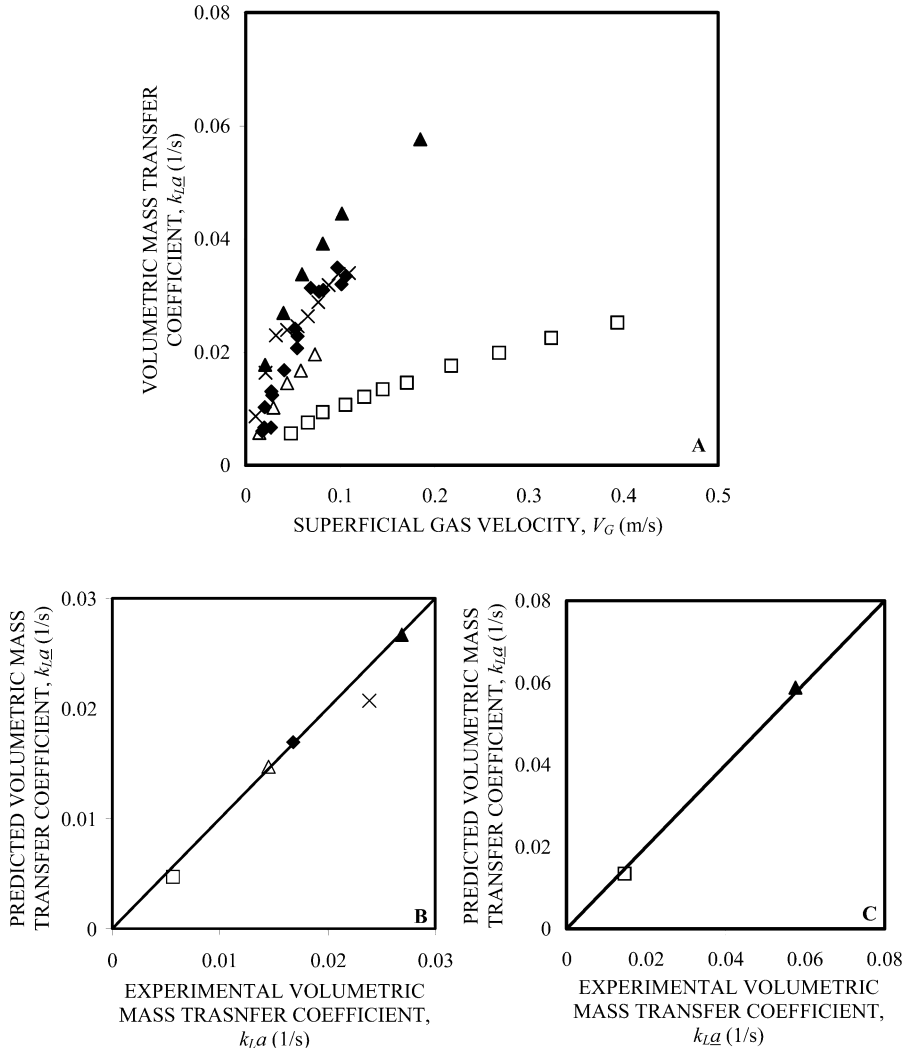

Figure 11. (A) k_La values for viscous Newtonian systems, experimental data of Yoshida and Akita[21] (◆, air−(aqueous glycerol solution)), Vandu and Krishna[57] (□, air−(tellus oil)), Koide et al.[12] (▲, air−(aqueous glycol solution)), Merchuk and Ben-Zvi[56] (×, air−(aqueous glycerol solution)), and Ozturk et al.[51] (Δ, air−(aqueous glycol solution)). (B) Parity plot for $V_G = 0.045$ m/s using SVR. (C) Parity plot for $V_G = 0.18$ m/s using SVR.

(eq 55) can be obtained from Gandhi et al.[5] However, for the present study, the optimal SVR parameters have been estimated using genetic algorithm for the first time. The GA-based optimization has been carried out, keeping the %AARE as the objective function to be minimized.

5.2.2. Hybrid GA-SVR Model. The detailed algorithm (Figure 1) for pursuing the same has been mentioned as follows:

The initial three steps of the algorithm are the same as those aforementioned for the SVR model, while the later part is discussed below.

(4) *Initial selection of the exponents and exponentially scaling of the features*: A set of the initial guess of the exponents *a*, *b*, *c*, ..., *n* to the individual features is randomly selected for the train data set.

$$x_1^a,\ x_2^b,\ x_3^c,\ \ldots,\ x_n^n \tag{59}$$

(5) *Linear scaling of the exponentially scaled features*: The exponentially scaled features are subjected to the conventional linear scaling from +1 to −1.

(6) *SVR prediction*: Subjecting the dually scaled data set for model prediction with the aid of already defined SVR model parameters to obtained the revised prediction of the target outputs (eq 55), y_{pred}.

(7) *Defining error objective function*: The difference between the actual and the predicted values of the target output ($y_{actual} - y_{pred}$), defined as the objective function (eq 58) for the GA-based optimization.

(8) *Defining the new set of optimal exponents using GA*: On the basis of the error objective function, the new population of the exponents is defined using GA (crossover and mutation of the existing exponents). These newly defined values of exponents are reconsidered for calculation and thereby repeating steps 4−8, until the termination criteria for the least error is achieved. Eventually, the optimization results into the optimal values of the exponents, meant for exponential scaling of the train data set.

In the current study, the MATLAB 7 environment was used for developing computer codes of genetic algorithm optimization by utilizing the Genetic Algorithm Toolbox. The optimal values of the exponents associated with the individual features obtained through GA are listed in Table 7.

5.3. Correlation for ϵ_G, k_La, and a. On the basis of the procedure as described by our previous paper[5] the final regression function is established which is represented by the number of support vectors, the name of the kernel used (in this study RBF), optimized parameters (C, γ, and ε) obtained from *k*-fold cross-validation procedure and the value of the bias term "*b*". All these parameters are considered in calculations for prediction of new output based on desired input features. The numbers of support vectors were obtained by running the SVR

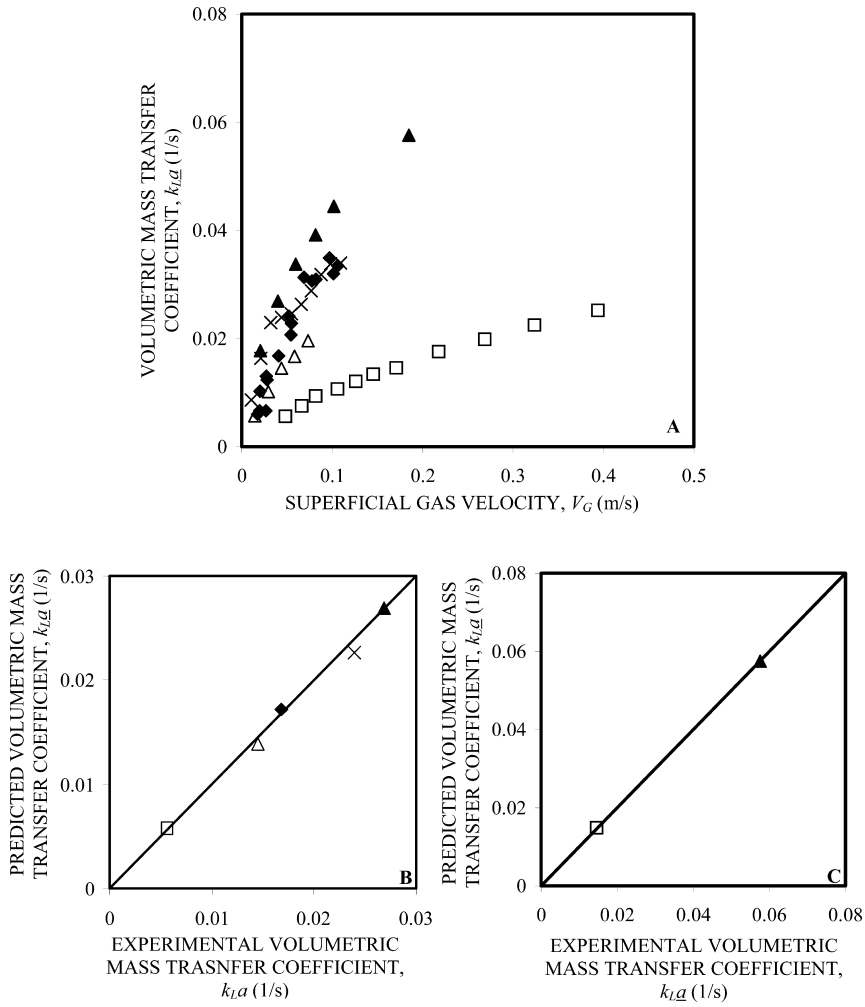

Figure 12. (A) $k_L\underline{a}$ values for viscous Newtonian systems, experimental data of Yoshida and Akita[21] (◆, air−(aqueous glycerol solution)), Vandu and Krishna[57] (□, air−(tellus oil), Koide et al.[12] (▲, air−(aqueous glycol solution)), Merchuk and Ben-Zvi[56] (×, air−(aqueous glycerol solution)), and Ozturk et al.[51] (Δ, air−(aqueous glycol solution)). (B) Parity plot for $V_G = 0.045$ m/s using SVR-GA. (C) Parity plot for $V_G = 0.18$ m/s using SVR-GA.

software using the procedure mentioned above. The number of support vectors along with the optimal value of the parameters (C, γ, and ε) for the individual data sets collected is summarized in Table 8. These values reported as in Table 8 are associated with the data set, wherein both the features as well as the target outputs are in scaled format. These optimal values have been developed by using the ε-SVR-based formalism, and the best values of C, ε, and γ were obtained by using the standard k-fold cross-validation procedure. The details of the procedure are provided in Gandhi et al.[5] For the case of hybrid GA-SVR model, the so-obtained optimal values of the exponents for each of the features using GA are also being considered for the calculation of the target outputs.

To facilitate the usage of the models devised, they have been made available on the web in the form of excel sheets. They are named as "GA-SVR_GH_BC_VN", "GA-SVR_GH_BC_VNN", "GA-SVR_MTC_BC_VN", "GA-SVR_MTC_BC_VNN", and "GA-SVR_AREA_BC_VNN". Here GH stands for overall gas hold-up, MTC stands for volumetric mass-transfer coefficient, and AREA stands for effective interfacial area, while VN stands for viscous Newtonian systems and VNN stands for viscous non-Newtonian systems. These tools can be downloaded from the web site http://www.esnips.com/web/UICT-NCL. In these tools for, e.g., "GA-SVR_MTC_BC_VN", one can insert the desired input parameters (16) and the cell named "*MTC predicted*" gives the value of the predicted output ($k_L\underline{a}$). The prediction is made on the basis of the procedure described in the earlier sections. The support vectors are listed in their scaled format in the sheet named "*support vectors* $k_L\underline{a}$" for $k_L\underline{a}$. The calculation of kernel elements is done in sheet named "*kernel elements* $k_L\underline{a}$" for $k_L\underline{a}$ by using eq 56. The above-mentioned sheets are password protected in order to ensure that the vital information within is not tampered. The summation of the product of the above-mentioned kernel elements and the corresponding nonzero Lagrange multiplier for each of the support vectors with addition of the bias term to it gives the predicted output as per eq 55. The predicted value is displayed in the cell named "*MTC predicted*" for $k_L\underline{a}$ in sheet "*SVR model* $k_L\underline{a}$". Similar methodology is followed for the other tools with $k_L\underline{a}$ being replaced by ϵ_G and $\underline{a}$ for overall gas hold-up and effective interfacial area, respectively.

6. Results and Discussion

For the optimal model parameters as mentioned in Table 8, parity plots are shown in Figure 2A and Figure 2B for viscous Newtonian and non-Newtonian systems, respectively, for overall gas hold-up, Figure 3A,B for viscous Newtonian and non-Newtonian systems, respectively, for volumetric mass-transfer coefficient, and Figure 4 for viscous non-Newtonian systems for effective interfacial area. It can be seen from these parity

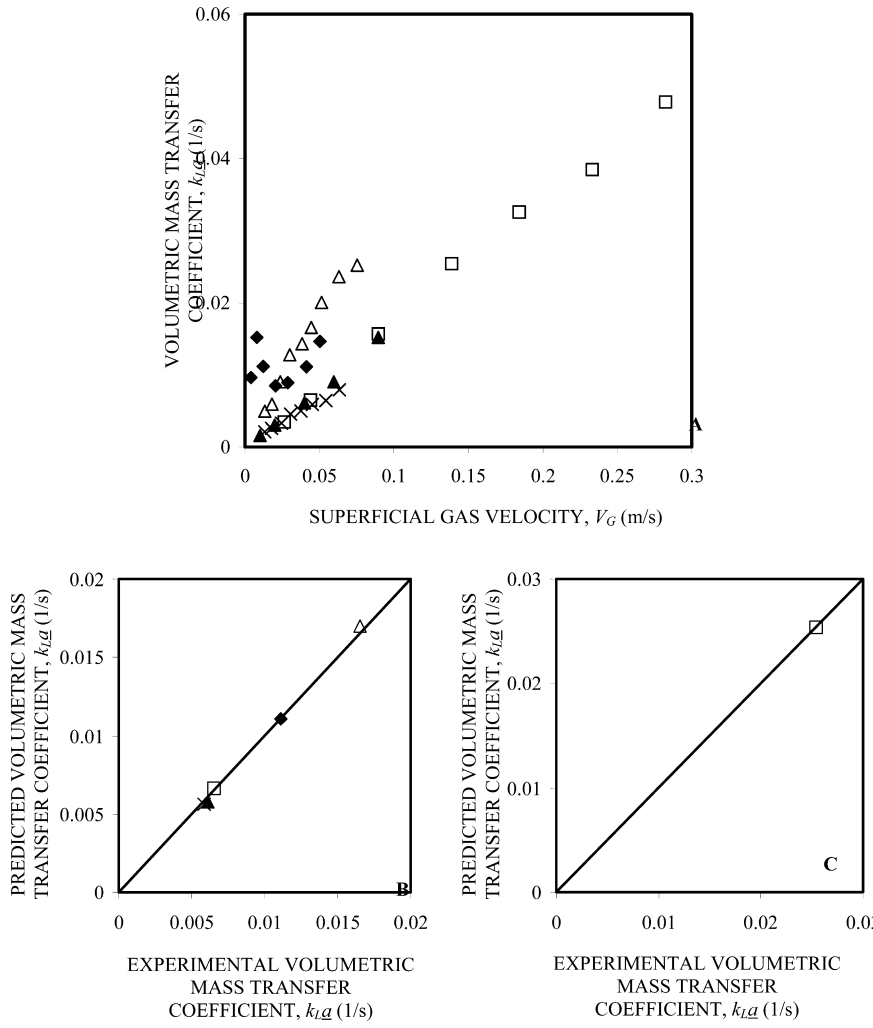

Figure 13. (A) k_La values for viscous non-Newtonian systems, experimental data of Deckwer et al.[42] (◆, air−(aqueous CMC solution)), Suh et al.[59] (□, air−(aqueous xanthan solution)), Kawase et al.[37] (Δ, air−(aqueous Carbopol solution)), Moo-Young and Kawase[46] (×, CO_2−(aqueous separan solution)), and Eickenbusch et al.[47] (▲, air−(aqueous hydroxypropyl guar gum solution)). (B) Parity plot for $V_G = 0.043$ m/s using SVR. (C) Parity plot for $V_G = 0.135$ m/s using SVR.

plots that a fairly good agreement is obtained between the experimental and predicted values.

6.1. SVR and Hybrid GA-SVR-Based Correlation Compared Against Literature Correlations. To evaluate the performance of the existing correlations as mentioned in Tables 1A,B, 2, and 3A,B, it was thought desirable to test these correlations against the data set collected and compare them with SVR and hybrid GA-SVR-based correlations. The comparison of the existing correlations with SVR- and hybrid GA-SVR-based correlations are summarized in Table 9 for the overall gas hold-up, Table 10 for volumetric mass-transfer coefficient, and Table 11 for effective interfacial area, respectively. It can be seen that all the correlations give poor predictions for the collected data sets although they were tested for the range for which these correlations have been proposed. The hybrid GA-SVR-based correlations for ϵ_G, k_La, and a show excellent agreement with the experimental values, better than any of the correlations previously published in the literature. Plots showing the performance of hybrid GA-SVR-based correlations for ϵ_G, k_La, and a against literature correlations have been uploaded on the web link mentioned above and can be accessed from the document named "graphs correlation viscous media".

6.2. Performance by SVR- and Hybrid GA-SVR-Based Correlations for Various Test Data Sets. The SVR-based models were also compared with data sets for which they were not trained, i.e., a test data set. The simulation conditions were selected in such a manner so as to see the effect of viscous gas−liquid systems and operating conditions on ϵ_G, k_La, and a. For this purpose SVR and hybrid GA-SVR simulations for the test data set were carried out, and the results of the simulations along with the range of the test data sets are summarized in Table 12. For testing SVR- and hybrid GA-SVR-based models for ϵ_G, the viscous Newtonian data set of De Swart and Krishna[65] and viscous non-Newtonian data set of Vatai and Tekic[39] were selected. For k_La, simulations were done at experimental conditions for the Newtonian data set and those of Buchholz et al.[41] for the non-Newtonian data set. Also, for a, the non-Newtonian data set of Schumpe and Deckwer[34] have been used for SVR-based simulations. The simulation results for SVR- and hybrid GA-SVR-based correlations are also shown in Figure 5A for viscous Newtonian systems for ϵ_G and k_La, in Figure 5B for viscous non-Newtonian systems for ϵ_G and k_La, and in Figure 6 for viscous non-Newtonian systems for a. It can be seen from the plots as well as from the results reported in Table

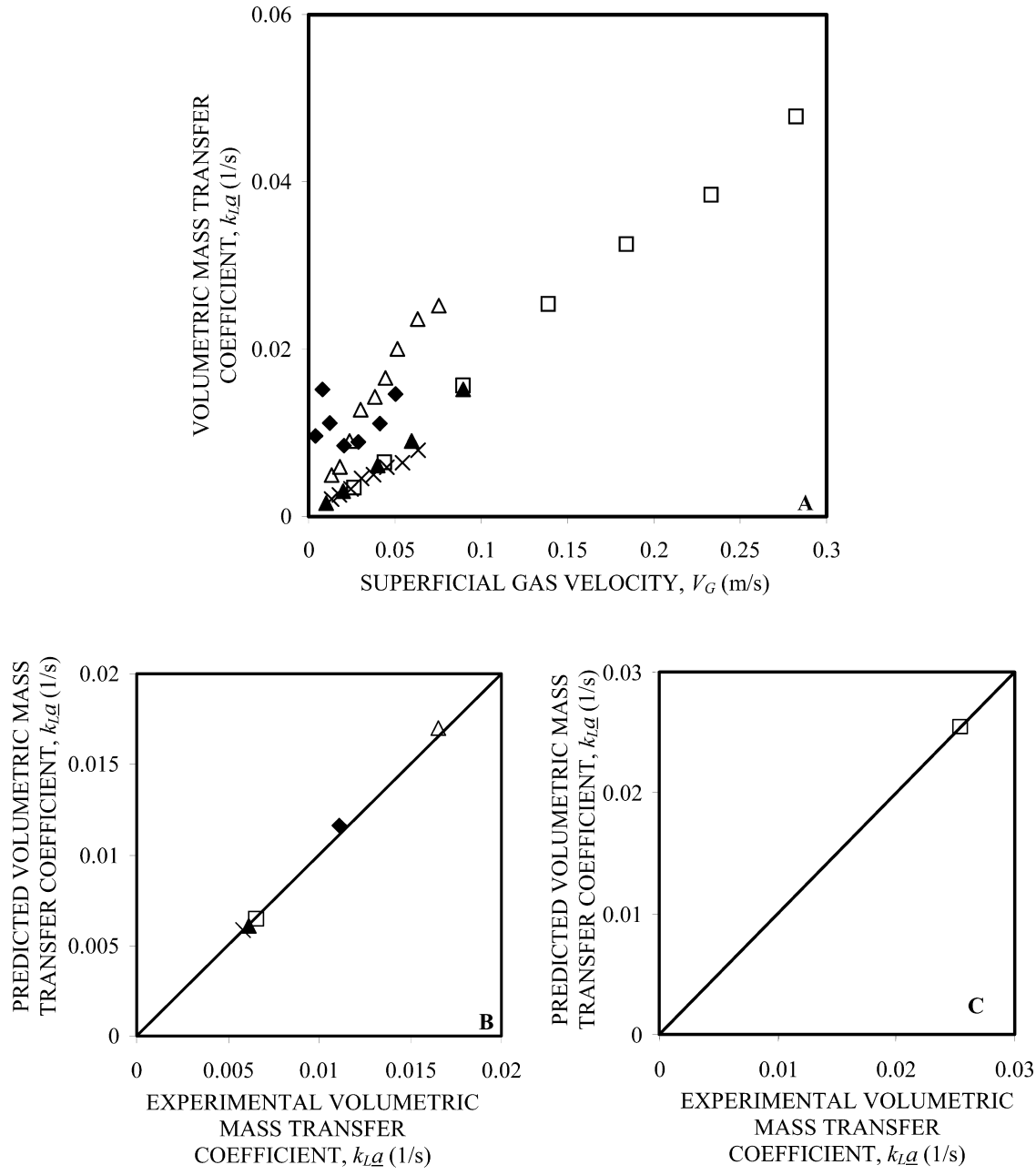

Figure 14. (A) k_La values for viscous non-Newtonian systems, experimental data of Deckwer et al.[42] (◆, air−(aqueous CMC solution)), Suh et al.[59] (□, air−(aqueous xanthan solution)), Kawase et al.[37] (Δ, air−(aqueous Carbopol solution)), Young and Kawase[46] (×, CO_2−(aqueous separan solution)), and Eickenbusch et al.[47] (▲, air−(aqueous hydroxypropyl guar gum solution)). (B) Parity plot for $V_G = 0.043$ m/s using SVR-GA. (C) Parity plot for $V_G = 0.135$ m/s using SVR-GA.

12 that excellent agreement between the experimental test data set and predictions by hybrid GA-SVR-based correlations can be obtained.

6.3. Parametric Sensitivity Analysis. To check the applicability of the SVR- and hybrid GA-SVR-based correlations for both the homogeneous and heterogeneous regimes, parametric sensitivity analysis has been carried out. For this purpose, a particular value of V_G was selected for each of the two regimes, homogeneous and heterogeneous. Thus, for the viscous Newtonian data set for ϵ_G, V_G was selected as 0.045 and 0.145 m/s for homogeneous and heterogeneous regimes, respectively. Figures 7A and 8A show the plot of the data set considered, and it can be seen that at the above two velocities wide variation in ϵ_G exists. For the homogeneous regime, ϵ_G varies from 0.0796 to 0.243 with the lowest value obtained by Kuncova and Zahradnik[28] while the highest value was obtained by Macchi et al.[30] Besides, data of Yoshida and Akita[21] and Vandu and Krishna[57] are also considered, where apart from variation in sparger geometry different gas and liquid properties are also responsible for variation in k_La. Similarly, for the heterogeneous regime, ϵ_G varies from 0.221 to 0.295. At such high gas velocities, only the data set of Macchi et al.[30] was applicable, which is shown in increasing order with three different gases employed by them. Parity plots capturing the effects of all above-mentioned parameters are shown in Figure 7B,C for $V_G = 0.045$ m/s and $V_G = 0.145$ m/s, respectively, for the SVR-based model. Parts B and C of Figure 8 show parity plots for $V_G = 0.045$ m/s and $V_G = 0.145$ m/s, respectively, for the hybrid GA-SVR-based model. It can be seen from the plots that the hybrid GA-SVR-based model gives better agreement between the experimental and predicted values than SVR-based model.

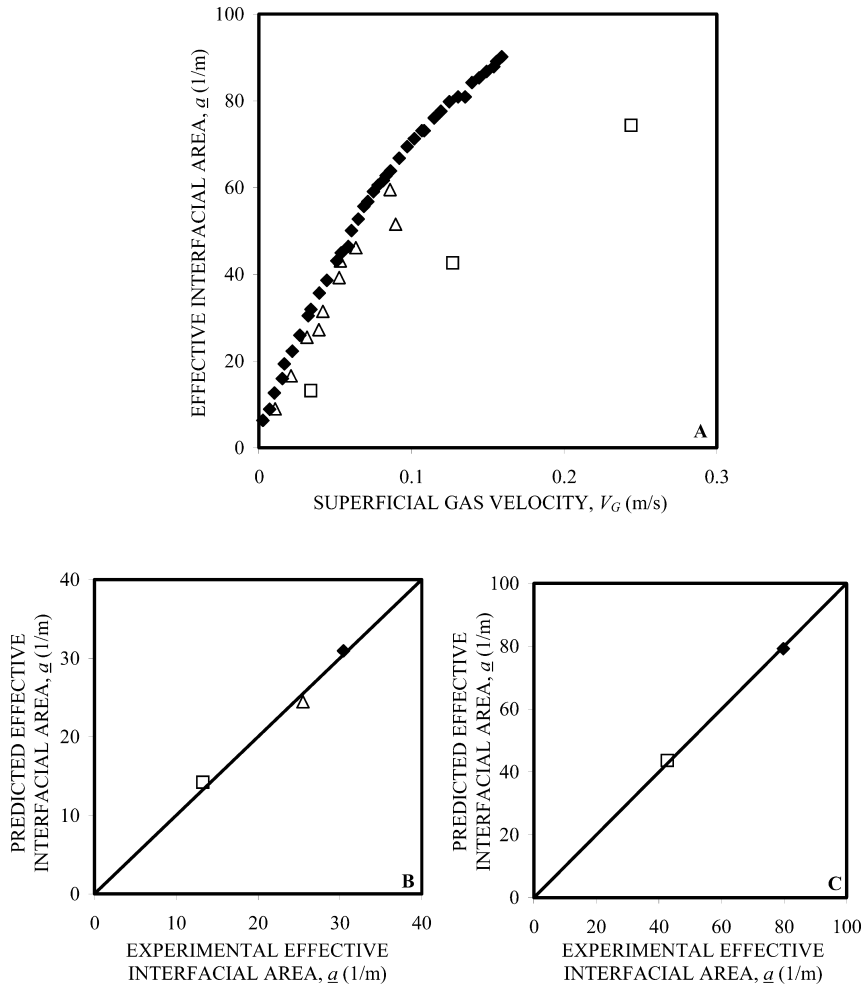

Figure 15. (A) a values for viscous non-Newtonian systems, experimental data of Schumpe and Deckwer[34] (◆, air−(aqueous CMC dissolved in 0.8 M NA_2SO_3 solution)), Godbole et al.[31] (□, air−(aqueous CMC dissolved in 0.8 M NA_2SO_3 solution)), and Popovic and Robinson[45] (Δ, air−(aqueous CMC dissolved in 0.8 M NA_2SO_3 solution)). (B) Parity plot for $V_G = 0.03$ m/s using SVR. (C) Parity plot for $V_G = 0.12$ m/s using SVR.

Similarly for non-Newtonian systems for ϵ_G, simulations were carried out at two velocities (0.041 and 0.145 m/s). Figures 9A and 10A show the wide variation in ϵ_G at the two velocities selected. For the lower gas velocity, ϵ_G varies from 0.0457 to 0.1, while for higher gas velocity ϵ_G varies from 0.114 to 0.222. In both cases, the minimum value was obtained by Haque et al.,[43] while the maximum value was obtained by Fransolet et al.[32] Besides, data sets of Eickenbusch et al.,[47] Deckwer et al.,[42] Kawase et al.,[37] and Popovic and Robinson[45] have also been considered, as can be seen from Figures 9A and 10A. Here, the major variation is due to variation in liquid viscosity and also sparger geometry. These effects on ϵ_G have been captured well as can be seen from the parity plots, Figure 9B,C, for $V_G =$ 0.041 and 0.145 m/s, respectively, for the SVR-based model. However, parity plots shown in Figure 10B,C for $V_G = 0.041$ and 0.145 m/s, respectively, for the hybrid GA-SVR-based model give more enhanced predictions than SVR-based models.

Variation in the Newtonian data set for k_La is shown in Figures 11A and 12A, and simulations were carried out at V_G $= 0.045$ and 0.18 m/s. Here at the lower gas velocity, k_La varies from 0.0057 to 0.0269 1/s, while, at higher gas velocity, k_La varies from 0.0146 to 0.0576 1/s. In both cases, the minimum values were obtained by Vandu and Krishna,[57] while maximum values were obtained by Koide et al.[12] The data sets of Yoshida and Akita,[21] Merchuk and Ben-Zvi,[56] and Ozturk et al.[51] have also been reported in Figures 11A and 12A. Here the variations can be attributed primarily to sparger geometry and also varying liquid properties. Parity plots showing the performance of SVR-based correlations for such data sets are shown in Figure 11B,C for $V_G = 0.045$ and 0.18 m/s, respectively, while performance of hybrid GA-SVR-based correlations is shown in Figure 12B,C for $V_G = 0.045$ and 0.18 m/s, respectively. It can be seen from the parity plots that an excellent agreement between the experimental and predicted values is obtained for hybrid GA-SVR-based model as compared to the SVR-based model.

For the non-Newtonian data set for k_La, simulations were performed at $V_G = 0.043$ and 0.145 m/s with the variation at these two velocities in k_La values shown in Figures 13A and 14A. It can be seen from these figures that at the lower gas velocity k_La varies from 0.0058 to 0.011 1/s, while at higher gas velocity there is only one point obtained by Suh et al.[59] The lower value was obtained by Kawase et al.,[37] while the higher value was obtained by Deckwer et al.[42] Besides, the experimental data set of Suh et al.,[59] Moo-Young and Kawase,[46] and Eickenbusch et al.[47] are also shown in Figures 13A and 14A. The major variation in k_La values at the two velocities can be attributed to variation in liquid viscosity and sparger geometry. These effects on k_La have been captured well by the SVR-based model, as can be seen from the parity plots Figures 13B and 14C for $V_G = 0.043$ and 0.145 m/s, respectively. However, hybrid GA-SVR-based models give enhanced predictions for the same data sets, as can be seen from the parity plots Figure 14B,C for $V_G = 0.043$ and 0.145 m/s, respectively.

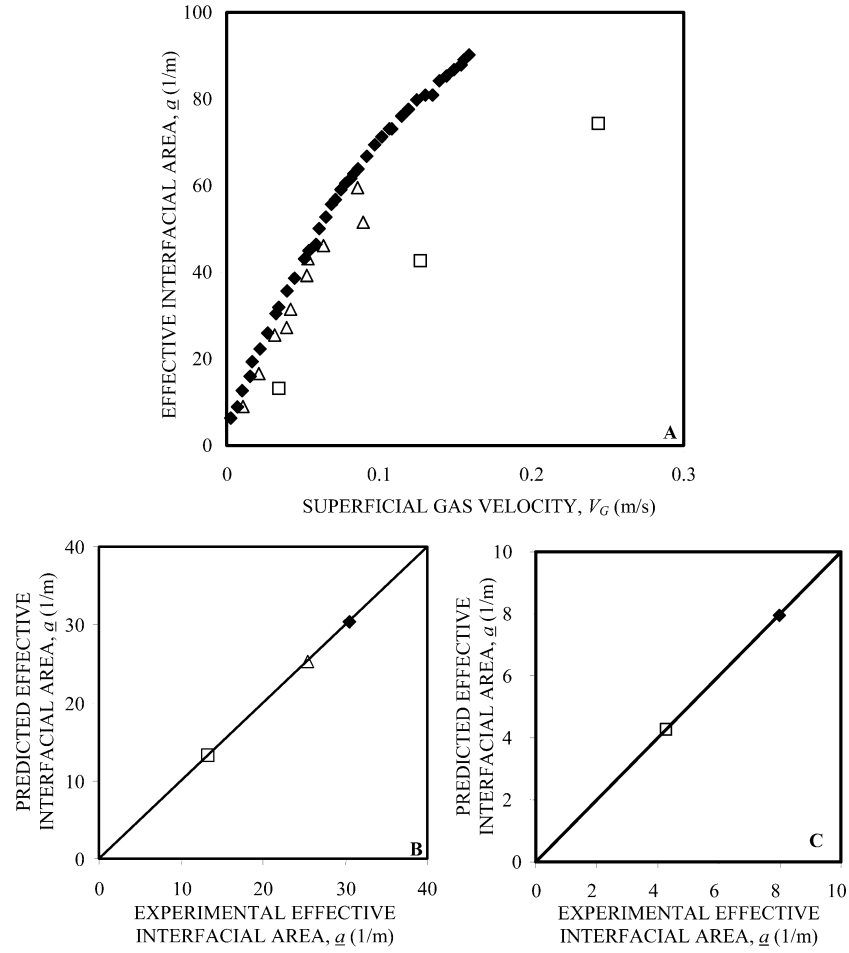

Figure 16. (A) $\underline{a}$ values for viscous non-Newtonian systems, experimental data of Schumpe and Deckwer[34] (◆, air−(aqueous CMC dissolved in 0.8 M NA_2SO_3 solution)), Godbole et al.[31] (□, air−(aqueous CMC dissolved in 0.8 M NA_2SO_3 solution)), and Popovic and Robinson[45] (Δ, air−(aqueous CMC dissolved in 0.8 M NA_2SO_3 solution)). (B) Parity plot for $V_G = 0.03$ m/s using SVR-GA. (C) Parity plot for $V_G = 0.12$ m/s using SVR-GA.

Similar analysis was carried out for $\underline{a}$ with simulations carried out at 0.03 and 0.12 m/s. The variation in experimental values at the two velocities is shown in Figures 15A and 16A. At the lower velocity, $\underline{a}$ varies from 13.43 to 30.46 m^{-1}, while at higher velocity $\underline{a}$ varies from 42.635 to 79.8 m^{-1}. The minimum values for both velocities were obtained by Godbole et al.,[31] while maximum values were obtained by Schumpe and Deckwer.[34] Besides, experimental data of Popovic and Robinson[45] are also reported in Figures 15A and 16A. The scatter in values of $\underline{a}$ can be attributed to variations in liquid viscosity and also sparger geometry. Parity plots for the same are shown in Figure 15B,C for $V_G = 0.03$ and 0.12 m/s, respectively, for the SVR-based model and in Figure 16B,C for $V_G = 0.03$ and 0.12 m/s, respectively, for the hybrid GA-SVR-based model. It can be seen from the parity plots that excellent agreement between the experimental and predicted values can be obtained by the hybrid GA-SVR-based model.

7. Conclusions

From the above discussion we can conclude that the hybrid GA-SVR-based correlations show remarkable improvement in predicting volumetric mass-transfer coefficient, effective interfacial area, and overall gas hold-up for viscous Newtonian and non-Newtonian systems as compared to other types of empirical and semiempirical correlations available in literature. The hybrid GA-SVR-based correlation for ϵ_G has a prediction accuracy of 0.994 and % AARE of 3.75% for the Newtonian data set and a prediction accuracy of 0.999 and % AARE of 1.65% for the non-Newtonian data set, while, for $k_L\underline{a}$, prediction accuracy was 0.983 and % AARE of 8.6% for the Newtonian data set, and a prediction accuracy of 0.998 and % AARE of 1.91% and for $\underline{a}$ prediction accuracy of 0.999 and % AARE of 1% for the non-Newtonian data set have been obtained. These correlations were also compared with all the literature correlations and were found to give comparatively much better predictions. The hybrid GA-SVR-based correlations also gave excellent predictions for the data sets for which they were not trained. When tested for the effect of individual parameters, GA-SVR-based correlations captured all the effects with excellent accuracy. Hence, the proposed hybrid GA-SVR-based correlations for ϵ_G, $k_L\underline{a}$, and $\underline{a}$ are expected to be useful in the design and scale-up of bubble column reactors for viscous Newtonian and non-Newtonian systems.

Nomenclature

$\underline{a}$ = effective interfacial area (m^2/m^3)
AARE = average absolute relative error $\{(1/N)\sum_{i=1}^{N} |(y_{pred} - y_{exptl})/(y_{exptl})|\}$
Bo = bond number ($gD^2\rho_L/\sigma_L$)
b = bias term
C = cost function
CC = correlation coefficient $\{\sum_{i=1}^{N}(y_{exptl(i)} - y_{exptl(mean)})(y_{pred(i)} - y_{pred(mean)})/[\sum_{i=1}^{N}(y_{exptl(i)} - y_{exptl(mean)})^2]^{1/2}[\sum_{i=1}^{N}(y_{pred(i)} - y_{pred(mean)})^2]^{1/2}\}$
d_B = surface to volume mean bubble diameter (m)
d_0 = sparger hole diameter (m)
d_s = sparger diameter (m)

D = column diameter (m)
De = Deborah number (relaxation time/observation time)
D_L = diffusivity of gas into liquid (m^2/s)
$f(x)$ = regression function
F = high dimensional feature space
Fr = Froude number ($V_G/(gD)^{1/2}$)
Ga = Galileo number ($gD^3\rho_L^2/\mu_L^2$)
g = acceleration due to gravity (m/s^2)
H_L = liquid height (m)
k_La = volumetric mass-transfer coefficient (1/s)
$K(x_i,x_j)$ = kernel function
K_d = sparger distribution coefficient
L = Lagrange function (dual form)
M_W = molecular weight of gas
n = flow behavior index
N_{gen} = number of generations
$N_{pop.}$ = initial population
N_{SV} = number of support vectors
N_0 = number of sparger holes
P = operating pressure (kPa)
P_{cross} = crossover rate
P_{mut} = mutation rate
Re = Reynolds number ($DV_G\rho_L/\mu_L$)
Sc = Schmidt number ($\mu_L/\rho_L D_L$)
Sh = Sherwood number ($k_La D^2/D_L$)
T = operating temperature (K)
V_G = superficial gas velocity (m/s)
V_L = superficial liquid velocity (m/s)
Wi = Weissenberg number
w = weight vector
x_i = ith input vector
y_i = target output corresponding to the ith vector
y_{pred} = predicted value of target output
y_{actual} = actual value of target output

Greek Letters

α_{ij}^* = Lagrange multipliers
$\gamma = 1/2\sigma^2$
γ_1 = shear rate
ε = loss function
ϵ_G = overall gas holdup
μ_{eff} = effective viscosity of liquid (Pa s)
μ_G = gas-phase viscosity (Pa s)
μ_L = liquid-phase viscosity (Pa s)
μ_W = viscosity of water (Pa s)
ρ_a = density of air (kg/m^3)
ρ_G = gas-phase density (kg/m^3)
ρ_L = liquid-phase density (kg/m^3)
ρ_W = density of water (kg/m^3)
σ = width of radial basis function (RBF) kernel
σ_L = liquid-phase surface tension (N/m)
σ_W = surface tension of water (N/m)
$\phi(x_i)$ = mapping function to high dimensional feature space for input vector **x**

Subscripts

exptl = experimental
G = overall gas phase
L = overall liquid phase
pred = predicted

Superscript

N = number of training data points

Abbreviations

ANN = artificial neural networks
GA = genetic algorithm
QP = quadratic programming
RBF = radial basis function kernel
SV = support vector
SVR = support vector regression
VN = viscous Newtonian
VNN = viscous non-Newtonian

Literature Cited

(1) Joshi, J. B.; Parasu Veera, U.; Prasad, Ch. V.; Phanikumar, D. V.; Deshpande, N. S.; Thakre, S. S.; Thorat, B. N. Gas hold-up structure in bubble column reactors. *Proc. Indian Natl. Sci. Acad.* **1998**, *64*, 441.

(2) Xie, T.; Ghiaasiaan, S. M.; Karrila, S. Artificial neural network approach for flow regime classification in gas-liquid fiber flows based on frequency domain analysis of pressure signals. *Chem. Eng. Sci.* **2009**, *59*, 2241.

(3) Shaikh, A.; Al-Dahhan, M. Development of an artificial neural network correlation for prediction of overall gas-holdup in bubble column reactors. *Chem. Eng. Process.* **2003**, *42*, 599.

(4) Desai, K.; Badhe, Y.; Tambe, S. S.; Kulkarni, B. D. Soft sensor development for fed-batch bioreactors using support vector regression. *Biochem. Eng. J.* **2006**, *27*, 225.

(5) Gandhi, A. B.; Joshi, J. B.; Jayaraman, V. K.; Kulkarni, B. D. Development of support vector regression (SVR)-based correlation for prediction of overall gas hold-up in bubble column reactors for various gas-liquid systems. *Chem. Eng. Sci.* **2007**, *62*, 7078.

(6) Brameier, M.; Banzhaf, W. A comparison of linear genetic programming and neural networks in medical data mining. *IEEE Trans. Evol. Comput.* **2001**, *5*, 17.

(7) Guo, H.; Jack, L. B.; Nandi, A. K. Feature generation using genetic programming with application to fault classification. *IEEE Trans. Syst. Man. Cybern. Cybern., Part B: Cybernetics* **2005**, *35*, 89.

(8) Ustun, B.; Melssen, W. J.; Oudenhuijzen, M.; Buydens, L. M. C. Determination of optimal support vector regression parameters by genetic algorithms and simplex optimization. *Anal. Chim. Acta* **2005**, *544*, 292.

(9) Nandi, S.; Badhe, Y.; Lonari, J.; Sridevi, U.; Rao, B. S.; Tambe, S. S.; Kulkarni, B. D. Hybrid process modeling and optimization strategies integrating neural networks/support vector regression and genetic algorithms: Study of benzene isopropylation on Hbeta catalyst. *Chem. Eng. J.* **2004**, *97*, 115.

(10) Istadi, N.; Amin, A. S. Hybrid artificial neural network−genetic algorithm technique for modeling and optimization of plasma reactor. *Ind. Eng. Chem. Res.* **2006**, *45*, 6655.

(11) Akita, K.; Yoshida, F. Gas holdup and volumetric mass transfer coefficient in bubble columns—Effects of liquid properties. *Ind. Eng. Chem. Process Des. Dev.* **1973**, *12*, 76.

(12) Koide, K.; Takazawa, A.; Komura, M.; Matsunaga, H. Gas hold-up and volumetric liquid-phase mass transfer coefficient in solid-suspended bubble columns. *J. Chem. Eng. Jpn.* **1984**, *17*, 459.

(13) Bach, H.; Pilhofer, T. Variation of gas hold-up in bubble columns with physical properties of liquids and operating parameters of columns. *Ger. Chem. Eng.* **1978**, *1*, 270.

(14) Hikita, H.; Asai, S.; Tanigawa, K.; Segawa, K.; Kitao, M. Gas hold-up in bubble columns. *Chem. Eng. J.* **1980**, *20*, 59–67.

(15) Sotelo, J. L.; Benitez, F. J.; Beltran-Heredia, J.; Rodriguez, C. Gas holdup and mass transfer coefficients in bubble columns. Porous glass-plate diffusers. *Int. Chem. Eng.* **1994**, *34*, 82.

(16) Godbole, S.; Honath, M.; Shah, Y. Hold-up structure in highly viscous Newtonian and non-Newtonian liquids in bubble column. *Chem. Eng. Commun.* **1982**, *16*, 119.

(17) Anabtawi, M.; Abu-Eishah, S.; Hilal, N.; Nabhan, M. Hydrodynamic studies in both bi-dimensional and three-dimensional bubble columns with a single sparger. *Chem. Eng. Process.* **2003**, *42*, 403.

(18) Urseanu, M.; Guit, R.; Stankeiwicz, A.; Kranenburg, G.; Lommen, J. Influence of operating pressure on the gas hold-up in bubble columns for high viscous media. *Chem. Eng. Sci.* **2003**, *58*, 697.

(19) Kazakis, N.; Papadopoulos, I.; Mouza, A. Bubble columns with fine pore sparger operating in the pseudo-homogenous regime: Gas hold-up prediction and a criterion for the transition to the heterogeneous regime. *Chem. Eng. Sci.* **2007**, *62*, 3092.

(20) Nedeltchev, S.; Schumpe, A. A new approach for the prediction of gas hold-up in bubble columns operated under various pressures in the homogeneous regime. *J. Chem. Eng. Jpn.* **2008**, *41*, 744.

(21) Yoshida, F.; Akita, K. Performance of gas bubble columns: Volumetric liquid phase mass transfer coefficient and gas holdup. *AIChE J.* **1965**, *11*, 9.

(22) Aoyama, Y.; Ogushi, K.; Koide, K.; Kubota, H. Liquid mixing in concurrent bubble columns. *J. Chem. Eng. Jpn.* **1968**, *1*, 158.

(23) Zahradnik, J.; Peter, R.; Kastanek, F. The effect of liquid phase properties on gas hold-up in bubble column reactors. *Collect. Czech. Chem. Commun.* **1987**, *52*, 336.

(24) Terasaka, K.; Tsuge, H. Mass transfer in highly viscous liquids in a bubble column with constant flow nozzles. *J. Chem. Eng. Jpn.* **1991**, *24*, 424.

(25) Daly, J.; Patel, S.; Bukur, D. Measurement of gas hold-ups and Sauter mean bubble diameters in bubble column reactors by dynamic gas disengagement method. *Chem. Eng. Sci.* **1992**, *47*, 3647.

(26) Chabot, J.; Lasa, H. Gas hold-ups and bubble characteristics in a bubble column operated at high temperature. *Ind. Eng. Chem. Res.* **1993**, *32*, 2595.

(27) Soong, Y.; Harke, F.; Gamwo, I.; Schehl, R.; Zarochak, M. Hydrodynamic study in a slurry bubble column reactor. *Catal. Today* **1997**, *35*, 427.

(28) Kuncova, G.; Zahradnik, J. Gas hold-up and bubble frequency in a bubble column reactor containing viscous saccharose solutions. *Chem. Eng. Process.* **1995**, *34*, 25.

(29) Zahradnik, J.; Kuncova, G.; Fialova, M. The effect of surface active additives on bubble coalescence and gas hold-up in viscous aerated batches. *Chem. Eng. Sci.* **1999**, *54*, 2401.

(30) Macchi, A.; Bi, H.; Grace, J.; Mcknight, C.; Hackman, L. Effect of gas density on the hydrodynamics of bubble columns and three-phase fluidized beds. *Can. J. Chem. Eng.* **2003**, *81*, 846.

(31) Godbole, S. P.; Schumpe, A.; Shah, Y. T.; Carr, N. L. Hydrodynamics and mass transfer in non-Newtonian solutions in a bubble column. *AIChE J.* **1984**, *30*, 213.

(32) Fransolet, E.; Crine, M.; Marchot, P.; Toye, D. Analysis of gas hold-up in bubble columns with non-Newtonian fluid using electrical resistance tomography and dynamic gas disengagement technique. *Chem. Eng. Sci.* **2005**, *60*, 6118.

(33) Lakota, A. Effect of highly viscous non-Newtonian liquids on gas hold-up in a concurrent upflow bubble column. *Acta Chim. Slov.* **2007**, *54*, 678.

(34) Schumpe, A.; Deckwer, W. D. Gas holdups, specific interfacial areas and mass transfer coefficients of aerated carboxymethyl cellulose solutions in a bubble column. *Ind. Eng. Chem. Process Des. Dev.* **1982**, *21*, 706.

(35) Devine, W.; Shah, Y.; Morsi, B. Liquid phase axial mixing in a bubble column with viscous non-Newtonian liquids. *Can. J. Chem. Eng.* **1985**, *63*, 195.

(36) Kawase, Y.; Moo-Young, M. Influence of non-Newtonian flow behavior on mass transfer in bubble columns with and without draft tubes. *Chem. Eng. Commun.* **1985**, *40*, 67.

(37) Kawase, Y.; Halard, B.; Moo-Young, M. Theoretical prediction of volumetric mass transfer coefficients in bubble columns for Newtonian and non-Newtonian fluids. *Chem. Eng. Sci.* **1987**, *42*, 1609.

(38) Haque, M.; Nigam, K.; Joshi, J. B. Hydrodynamics and mixing studies in highly viscous pseudo-plastic non-Newtonian solutions in bubble column. *Chem. Eng. Sci.* **1986**, *41*, 2321.

(39) Vatai, G.; Tekic, M. Gas hold-up and mass transfer in bubble columns with pseudoplastic liquids. *Chem. Eng. Sci.* **1989**, *44*, 2402.

(40) Schumpe, A.; Deckwer, W. Viscous media in tower bioreactors: Hydrodynamic characteristics and mass transfer properties. *Bioprocess Eng.* **1987**, *2*, 79.

(41) Buchholz, H.; Buchholz, R.; Lucke, J.; Schugerl, K. Bubble swarm behavior and gas absorption in non-Newtonian fluids in sparged columns. *Chem. Eng. Sci.* **1978**, *33*, 1061.

(42) Deckwer, W. D.; Nguyen-Tien, K.; Schumpe, A.; Serpemen, Y. Oxygen mass transfer into aerated CMC solutions in a bubble column. *Biotechnol. Bioeng.* **1982**, *24*, 461.

(43) Haque, M.; Nigam, K.; Viswanathan, K.; Joshi, J. B. Studies on gas hold-up and bubble parameters in bubble columns with (carboxymethyl) cellulose solutions. *Ind. Eng. Chem. Res.* **1987**, *26*, 86.

(44) Bando, Y.; Chaya, M.; Hamano, S.; Yasuda, K.; Nakamura, M.; Osada, K.; Matsui, M. Effect of liquid height on flow characteristics in bubble column using highly viscous liquid. *J. Chem. Eng. Jpn.* **2003**, *36*, 523.

(45) Popovic, M.; Robinson, C. Mass transfer studies of external-loop airlifts and a bubble column. *AIChE J.* **1989**, *35*, 393.

(46) Moo-Young, M.; Kawase, Y. Gas hold-up and mass transfer in a bubble column with viscoelastic fluids. *Can. J. Chem. Eng.* **1987**, *65*, 113.

(47) Eickenbusch, H.; Brunn, P.-O.; Schumpe, A. Mass transfer into viscous pseudoplastic liquid in large-diameter bubble columns. *Chem. Eng. Process.* **1995**, *34*, 479.

(48) Popovic, M.; Robinson, C. The specific interfacial area in external circulation-loop airlifts and a bubble column-II. Carboxymethyl cellulose/sulphite solution. *Chem. Eng. Sci.* **1987**, *42*, 2825.

(49) Nakanoh, M.; Yoshida, F. Gas absorption by Newtonian and non-Newtonian liquids in a bubble column. *Ind. Eng. Chem. Process Des. Dev.* **1980**, *19*, 190.

(50) Hikita, H.; Asai, S.; Tanigawa, K.; Segawa, K.; Kitao, M. The volumetric liquid-phase mass transfer coefficient in bubble columns. *Chem. Eng. J.* **1981**, *22*, 61.

(51) Ozturk, S. S.; Schumpe, A.; Deckwer, W. D. Organic liquids in a bubble column: Holdups and mass transfer coefficients. *AIChE J.* **1987**, *33*, 1473.

(52) Quicker, G.; Deckwer, W. D. Gas holdup and interfacial area in aerated hydrocarbons. *Ger. Chem. Eng.* **1981**, *4*, 363.

(53) Alvarez, E.; Sanjurjo, B.; Cancela, A.; Navaza, J. Mass transfer and influence of physical properties of solutions in a bubble column. *Trans. Inst. Chem. Eng.* **2000**, *78A*, 889.

(54) Lau, R.; Peng, W.; Velazquez-Vergas, L. G.; Yang, G. Q.; Fan, L. S. Gas−liquid mass transfer in high pressure bubble columns. *Ind. Eng. Chem. Res.* **2004**, *43*, 1302.

(55) Nedeltchev, S.; Jordan, U.; Schumpe, A. Correction of the penetration theory based on mass-transfer data from bubble columns operated in the homogenous regime under high pressure. *Chem. Eng. Sci.* **2007**, *62*, 6263.

(56) Merchuk, J.; Ben-Zvi, S. A novel approach to the correlation of mass transfer rates in bubble columns with non-Newtonian liquids. *Chem. Eng. Sci.* **1992**, *47*, 3517.

(57) Vandu, C.; Krishna, R. Volumetric mass transfer coefficients in slurry bubble columns operating in the churn-turbulent regime. *Chem. Eng. Process.* **2004**, *43*, 987.

(58) Fujie, K.; Tsuchiya, K.; Fan, L.-S. Determination of volumetric oxygen transfer coefficient by off-gas analysis. *J. Ferment. Bioeng.* **1994**, *77*, 522.

(59) Suh, I. S.; Schumpe, A.; Deckwer, W. D.; Kulicke, W. M. Gas-liquid mass transfer in the bubble column with viscoelastic liquid. *Can. J. Chem. Eng.* **1991**, *69*, 506.

(60) Moo-Young, M.; Kawase, Y. Gas hold-up and mass transfer in a bubble column with viscoelastic fluids. *Can. J. Chem. Eng.* **1987**, *65*, 113.

(61) Vapnik, V.; Golowich, S.; Smola, A. J. Support vector method for function approximation, regression estimation and signal processing. *Adv. Neural Inf. Process. Syst.* **1996**, *9*, 281.

(62) Smola, A. J.; Scholkopf, B. A tutorial on support vector regression. *Stat. Comp.* **2004**, *14*, 199.

(63) Goldberg, D. E. *Genetic algorithms in searching, optimization, and machine learning*; Addison-Wesley: Reading, MA, 1988.

(64) Chang, C. C.; Lin, C. J. LIBSVM: A library for support vector machines, http://www.csie.ntu.edu.tw/~cjlin/libsvm, 2001.

(65) De Swart, J. W. A.; Krishna, R. Influence of particles concentration on the hydrodynamics of bubble column slurry reactors. *Trans. Inst. Chem. Eng.* **1995**, *73A*, 308.

Received for review December 1, 2008
Revised manuscript received March 24, 2009
Accepted April 1, 2009

IE801834W